Land surface phenology from optical satellite measurement and CO_2 eddy covariance technique

Alemu Gonsamo,[1] Jing M. Chen,[1] David T. Price,[2] Werner A. Kurz,[3] and Chaoyang Wu[1]

Received 9 May 2012; revised 1 August 2012; accepted 4 August 2012; published 21 September 2012.

[1] Land surface phenology (LSP) is an integrative indicator of vegetation dynamics under a changing environment. Increasing amounts of remote sensing measurements and CO_2 flux observations offer unprecedented opportunities to quantify LSP phases at landscape scale. LSP start of season (SOS) and end of season (EOS) estimates are often based on the use of a single-purpose vegetation index derived from optical satellite data, characterized by poor performances in decoupling soil and snow cover dynamics from LSP cycles, as well as contrasting responses of the needleleaf and broadleaf forests in boreal ecosystems. We propose a new remote-sensing-based phenology index (PI) which combines the merits of normalized difference vegetation index (NDVI) and normalized difference infrared index (NDII) by taking the difference of squared greenness and wetness to remove the soil and snow cover dynamics from key vegetation LSP cycles. We have cross-validated the remote-sensing-based LSP dates with those of CO_2 flux observations from 11 selected tower sites across Canada and the United States consisting of needleleaf forests, broadleaf forests, and croplands. The results indicate that PI estimates the SOS and EOS dates better than NDVI when compared to the LSP dates from CO_2 flux measurements (reduced RMSE, bias and dispersions, and higher correlation). PI-based SOS and EOS estimates are in good agreement with those derived from CO_2 flux measurements with mean bias comparable to the temporal resolution of the high-quality, 8-day composite satellite measurements. Finally, PI also shows a smoother time series compared to NDVI and NDII.

Citation: Gonsamo, A., J. M. Chen, D. T. Price, W. A. Kurz, and C. Wu (2012), Land surface phenology from optical satellite measurement and CO_2 eddy covariance technique, *J. Geophys. Res.*, *117*, G03032, doi:10.1029/2012JG002070.

1. Introduction

[2] Phenology has become a key research topic in the understanding of the effects of climate change on animal and plant populations [*Parmesan*, 2006]. Plant phenology is the study of the timing of recurring biological events in the plant world, the causes of their timing with regard to biotic and abiotic forces, and the interrelation among phases of the same or different species—all of which are critical subjects in global change sciences [*Lieth*, 1974]. Plant phenology is often studied at different scales, ranging from plant organs (first leaf and first flower), individual plants (leaf expansion and flowering), and communities of vegetation up to entire landscapes. Among the different scales, land surface phenology (LSP), which is measurable by earth observation satellites [*Dunn and de Beurs*, 2011; *Ganguly et al.*, 2010; *Liang et al.*, 2011; *Sakamoto et al.*, 2010], is an integrative indicator of vegetation dynamics in a changing environment [*Bradley et al.*, 2011; *Brown et al.*, 2010; *Jeong et al.*, 2012; *Zhang et al.*, 2007]. Recent attempts also show extraction of LSP dates from CO_2 flux observations [*Noormets et al.*, 2009; *Richardson et al.*, 2010; *Richardson et al.*, 2012] and ground networks of web-cams [*Sonnentag et al.*, 2012], although objective methods to extract the LSP dates have yet to be developed. LSP is defined after *de Beurs and Henebry* [2004] as the study of the timing of recurring seasonal pattern of variation in vegetated land surfaces observed from synoptic sensors [*Gonsamo et al.*, 2012]. Changes in LSP events have the potential to broadly impact terrestrial ecosystems and human societies, by altering the timing of, for example, global carbon, water, and nitrogen cycles, interspecific interactions both among plants and between plants and insects, crop production, frost damage, pollination seasons, and spreading diseases [*Menzel and Fabian*, 1999; *Menzel et al.*, 2006; *Schwartz*, 1998; *Schwartz and Reiter*, 2000; *White et al.*, 1999; *White et al.*, 2009]. Despite the fact that LSP has emerged as an important focus for ecological and global change researches, there are still large lingering uncertainties related to the determination of the key phenological phases such as: start of growing season

[1]Department of Geography and Program in Planning, University of Toronto, Toronto, Ontario, Canada.
[2]Northern Forestry Centre, Canadian Forest Service, Natural Resources Canada, Edmonton, Alberta, Canada.
[3]Pacific Forestry Centre, Canadian Forest Service, Natural Resources Canada, Victoria, British Columbia, Canada.

Corresponding author: A. Gonsamo, Department of Geography and Program in Planning, University of Toronto, Room 5047, Sidney Smith Hall, 100 St. George St., Toronto, Ontario M5S 3G3, Canada. (gonsamoa@geog.utoronto.ca)

0148-0227/12/2012JG002070

(SOS) and end of growing season (EOS) [*Morisette et al.*, 2009; *Schwartz and Hanes*, 2010; *White et al.*, 2009].

[3] Global warming [*Intergovernmental Panel on Climate Change*, 2007] has altered the phenology and distribution of many plant and animal species, resulting in distinct changes from individuals to whole communities [*Walther et al.*, 2002]. For example, elevated temperatures have contributed to advanced events such as leaf unfolding [*Menzel and Fabian*, 1999], flowering [*Fitter and Fitter*, 2002], and leaf emergence [*Roy and Sparks*, 2000]. There have also been reports of delays in leaf fall, leading to longer growing seasons due to late autumns as well as earlier springs [*Delbart et al.*, 2008; *Menzel and Fabian*, 1999; *Menzel et al.*, 2006; *Parmesan*, 2006]. Nevertheless, hypotheses concerning the way global change is currently altering the timing of seasonal events mostly originate from sampling protocols dealing with only a few species surveyed intensively at relatively few study sites. Phenological controls of biotic and abiotic forces, and the interrelation among phases of the same or different species due to the changing climate should also be studied at the landscape scale in order to increase our understanding of large-scale global change. While the observed patterns are related to biological phenomena, LSP is distinct from traditional definitions of plant phenology, which refer to specific life-cycle events, and are based on in situ observations of individual plants or species [*Morisette et al.*, 2009]. LSP provides integrative information at moderate to coarse spatial resolutions, which relate to the timing of vegetation growth, senescence, dormancy, and associated surface phenomena at seasonal and interannual scales. Although LSP is strongly associated with trees and plants with deciduous leaves, boreal evergreen needleleaf forest (ENF) also shows a distinct LSP cycle. Here, we define the phenology of boreal ENF as seasonal development in "greenness" due to changes in canopy biochemistry, production of new needles by canopy species, photoperiod, development of understory vegetation, snowmelt, soil thaw, canopy thaw or any of these factors contributing the most for the early increase and late decrease of greenness. In seasonally frozen boreal ENF where vegetation productivity is constrained by low temperatures and plant-available moisture, increase in greenness primarily coincides with springtime canopy thaw [*Frolking et al.*, 1999; *Harazono et al.*, 2003; *Jarvis and Linder*, 2000; *McDonald et al.*, 2004]. In boreal ENFs, photosynthesis occurs prior to snowmelt if canopy temperatures are thawed, since solar irradiance is near the seasonal maximum. During the later stage of the growing season in the fall, potential greenness of boreal ENF is substantially reduced by decreasing photoperiod giving distinct LSP cycles.

[4] Optical satellite observations of land surface reflectances and their combination in the form of vegetation indices (VIs) are associated with the biophysical and biochemical properties of vegetation. The NOAA AVHRR archive of normalized difference vegetation index (NDVI) data is the longest time series for LSP studies, and the results from the analysis of AVHRR-based NDVI revealed significant changes in spring phenology of vegetation during the 1980s and 1990s [*Myneni et al.*, 1997]. Although the study of LSP using satellite observation is becoming a mature area of research, there are still several impeding problems, such as atmospheric interference in the satellite reflectance, NDVI insensitivity and noise [*Huete et al.*, 1994, 2002; *Huete and Jackson*, 1988], and difficulties of extracting the exact SOS and EOS dates from satellite time series, to mention but a few [see intercomparison review in *White et al.*, 2009; *Schwartz and Hanes*, 2010]. Another major problem is the lack of biome-scale ground phenological data that could be effectively compared with satellite measurements using a common scale [*Cleland et al.*, 2007]. Even where ground phenology data exist, they are usually point-based observations, which are hardly comparable with optical remote sensors that integrate over larger areas. Continuous flux measurements from CO_2 eddy covariance techniques, although barely exploited for phenological studies, offer an unprecedented opportunity to quantify phenological phases at the landscape level [e.g., *Noormets et al.*, 2009; *Gu et al.*, 2009; *Xiao et al.*, 2009; *Richardson et al.*, 2010; *Wu et al.*, 2012]. The large volumes of satellite optical observations and CO_2 flux measurements present an untapped potential to cross-validate the LSP phases as observed by synoptic sensors over the same landscape scale. Another development is the use of digital webcam images to track the LSP on ground [*Richardson et al.*, 2007]. This has been proven to be useful in validating the satellite remote sensing SOS estimates, although the major question of how successfully we can capture the slow browning EOS and phenologically relevant information remains [*Sonnentag et al.*, 2012].

[5] A survey of late twentieth- and early twenty-first-century phenology literature for North America highlights the conflicting SOS and EOS results across approaches and data sets obtained from satellite measurements, due in large part to the problems associated with LSP methodologies [*Schwartz and Hanes*, 2010; *White et al.*, 2009]. Scientists have found contrasting trends in North America: earlier SOS only across mixed boreal regions with later EOS in southeastern Canada during 1982–2003 [*Reed*, 2006]; earlier SOS everywhere except the southeastern U.S. during 1982–2003 [*Zhang et al.*, 2007]; no overall continental trend in SOS and delayed EOS during 1980–2002 [*Piao et al.*, 2007]; or longer growing season in the high Arctic and no changes across the forest regions during 1981–2003 [*Goetz et al.*, 2005], but almost no trends in SOS during 1981–2003 in the high Arctic [*Bunn and Goetz*, 2006]. Uncertainties in interpreting NDVI for phenology study arise from limitations such as contaminations by background reflectances from soil, leaf litter, dead branches, snow, soil thaw, snow thaw, and shadows, which also have distinct seasonal dynamics often misinterpreted as vegetation LSP. The findings from a detailed methodology comparison [*White et al.*, 2009] indicate that given NDVI data with identical duration, satellite correction scheme, geographic region, compositing scheme, and spatial resolution, SOS estimates differed in terms of average day of year (DOY) by more than one month, variability by more than two weeks, retrieval ability by more than one third, and ordinal ranking by latitude and ecoregion across methods. This brings into question the often illusive hopes of remote sensing and global change research communities that SOS estimation methods may have consistent ordinal behavior and may simply be detecting different portions of the annual vegetation phenological developmental cycle. *White et al.* [2009] have concluded that there is no rational evidence for supporting one method over another and to expect consistent ordinal behavior across and within method and ecoregion. Furthermore, detecting the LSP in

boreal regions is difficult as the NDVI increase corresponds to the beginning of snowmelt. Thanks to the shortwave-infrared (SWIR) spectral band, which is sensitive to land surface moisture, researchers have started using the normalized difference infrared index (NDII) for LSP studies [*Delbart et al.*, 2005]. NDII is promising to decouple the snow effect from LSP cycles. In late spring it decreases in concomitance with snowmelt before increasing due to vegetation development. In autumn NDII decreases because of senescence and successively increases due to snow accumulation. However, NDII-based LSP studies do not work well in boreal needleleaf vegetation where there is overlap of snowmelt and green-up, and in conditions of abrupt increase in soil moisture before green-up. This indicates that for LSP studies, NDVI and NDII are useful complements for simultaneous decoupling of seasonal dynamics of soil, land surface moisture and snow effects from vegetation LSP cycles.

[6] Therefore, the main contribution of the current study is to evaluate the integrative use of NDVI and NDII for vegetation LSP studies across temperate and boreal broadleaf forests, boreal needleleaf forest, and croplands. In this paper, we present and expand methodologies for deriving phenology metrics from optical satellite measurements and CO_2 eddy covariance observations. Specifically, we present (1) a new and improved phenology index (PI) from optical satellite data, (2) objective method to extract SOS and EOS from CO_2 eddy covariance observations, (3) an assessment of the potential of satellite observations to estimate slow browning EOS, and (4) a comprehensive comparison of SOS and EOS estimates from remote sensing and eddy covariance CO_2 measurements. The cross validation of SOS and EOS dates as estimated from the two independent observations fills the scaling gap observed in the existing validation activities of LSP metrics. Moreover, assessment of methodologies for estimating EOS is essential since previous studies mostly focus on SOS and recent findings are showing that forest carbon budget is governed more by EOS than SOS due to autumn respiration [*Piao et al.*, 2008].

2. Data

2.1. MODIS 500 m Reflectance Data

[7] We used the red (620–670 nm), near-infrared (NIR: 841–875 nm), and shortwave-infrared (SWIR: 1628–1652 nm) surface reflectance product (MOD09A1) from the Moderate Resolution Imaging Spectroradiometer (MODIS) satellite sensor. In the production of MOD09A1, atmospheric corrections for Rayleigh, ozone, stratospheric aerosols, and water vapor effects are implemented [*Vermote and Vermeulen*, 1999]. The MOD09A1 product is produced in 8-day "maximum quality" composites in 500 m pixels, choosing observations with minimal cloud cover, and near-nadir views. We acquired the MOD09A1 surface reflectance product in a form of ASCII subsets for selected CO_2 flux tower sites from the DAAC database at the Oak Ridge National Laboratory (http://daac.ornl.gov/MODIS/). We have extracted the red, NIR, and SWIR reflectances and the exact acquisition date for a single 500 m pixel at each flux tower site for period spanning from January 1st 2000 to December 31st 2009.

2.2. Site Description and CO_2 Flux Measurement

[8] We used CO_2 flux data from 11 forest and agricultural tower sites in the Canadian Carbon Program (CCP) and AmeriFlux networks (Table 1). The long-term records for 3 boreal evergreen needleleaf forest (ENF), 1 boreal deciduous broadleaf forest (DBF), 4 temperate deciduous broadleaf forest (DBF), and 3 agricultural cropland (CL) sites represent a wide diversity in regions, climate, species compositions, and crop management across North America (Figure 1; for detailed vegetation characteristics, see Table 1).

[9] The three BOReal Ecosystem–Atmosphere Study (BOREAS) boreal ENF sites are predominantly Black Spruce, an important tree species accounting for over 70% of boreal forest cover in Canada. The Manitoba Northern Old Black Spruce Site (CA-NOBS) is located near to the northern limit of closed canopy forest with average tree height of 10.6 m, mean annual air temperature of −3.2°C, and mean annual precipitation of 517 mm [*Dunn et al.*, 2007]. The Saskatchewan Southern Old Black Spruce (CA-SOBS) is located toward the southern edge of the boreal forest, comprising mostly Black Spruce, with approximately 15% deciduous larch with tree heights below 15 m, mean annual air temperature of +0.4°C, and mean annual precipitation of 467 mm [*Bergeron et al.*, 2007]. The Quebec Eastern Old Black Spruce (CA-EOBS) lies in the commercial boreal forest of Canada with mean annual air temperature of −0.36°C, mean annual precipitation of 962 mm, and mean tree height of 13.8 m [*Bergeron et al.*, 2007]. The Saskatchewan Old Aspen (CA-OA) site is also a BOREAS study site representing the only boreal DBF flux tower site over Canada, importantly located in a transitional zone between boreal forest and grassland representing the largest dominant and co-dominant overstory broadleaf tree species over the North American boreal zone, characterized by mean annual air temperature of 0.4°C, and mean annual precipitation of 467 mm and mean tree height of 21 m [*Barr et al.*, 2004]. All of the 4 CCP flux tower sites are characterized by strong seasonal patterns of snow, land surface moisture, and leaf development dynamics.

[10] The Wisconsin Willow Creek (U.S.-WCR) and Wisconsin Lost Creek (U.S.-Los) sites are part of the Chequamegon Ecosystem-Atmosphere Study (ChEAS) consisting of an upland mature temperate deciduous forest and Alder-willow shrub wetland, respectively with cold winter and seasonal snow cover, and mean annual precipitation of 790 mm [*Cook et al.*, 2004]. U.S.-WCR has mean canopy height of 24 m, whereas U.S.-Los has 2 m shrub overstory which is classified as DBF in IGBP vegetation classification, and in this paper for consistency. The Indiana Morgan Monroe State Forest (U.S.-MMS) is a secondary temperate successional DBF forest located within the maple-beech to oak hickory transition zone, with a canopy height of 25–27 m, 29 tree species identified in the vicinity of the tower site, mean annual precipitation of 871–1336 mm, mean air temperature of 12.4°C with mild winter and rare snowfall [*Dragoni et al.*, 2011]. The Michigan Biological Station (U.S.-UMB) site is located in the transition zone between the mixed hardwood and boreal forests consisting of deciduous overstory with a mean canopy height of 20 m, mean air temperature of 6.2°C, mean annual precipitation of 750 mm, and seasonal snow covers [*Nave et al.*, 2011]. The three agricultural cropland flux tower sites are from the University of Nebraska Agricultural Research and Development Center near Mead, Nebraska, all located within 1.6 km of each other. Mean annual temperature is 11.1°C and precipitation

Table 1. Detailed Description of CO_2 Flux Tower Sites[a]

Site ID	Site Name	Land Cover	Vegetation Description	Latitude/Longitude	Data Year	References
CA-NOBS	Manitoba Old Black Spruce	ENF	161-year-old Black Spruce with occasional larch overstory in poorly drained areas with Feather Moss, Sphagnum Moss, Labrador Tea, Vaccinium, and willows understory	55.8796 / −98.4808	2001–2008	*Dunn et al.* [2007]
CA-EOBS	Quebec Eastern Old Black Spruce	ENF	100–110-year-old Black Spruce and Jack Pine overstory with Feather Moss understory	49.6925 / −74.3420	2004–2009	*Bergeron et al.* [2007]
CA-SOBS	Saskatchewan Old Black Spruce	ENF	129-year-old Black Spruce overstory with Feather Moss and Labrador Tea understory	53.98717 / −105.1178	2001–2009	*Bergeron et al.* [2007]
CA-OA	Saskatchewan Old Aspen	DBF	90-year-old Aspen with a few Balsam Poplar and thick Hazel understory	53.6289 / −106.1978	2001–2009	*Barr et al.* [2004]
U.S.-WCR	Wisconsin Willow Creek	DBF	55–90-year-old Sugar Maple dominated with American Basswood and Green Ash overstory; and overstory saplings, Eastern Leatherwood, Northern Maidenhair, Western Bracken Fern and Blue Cohosh understory growing in poorly drained soil	45.8059 / −90.0799	2000–2003 2005–2006	*Cook et al.* [2004]
U.S.-MMS	Indiana Morgan Monroe State Forest	DBF	70–90-year-old mixed hardwoods secondary growth with Tulip Poplar, White Oak, Red Oak, and Sugar Maple dominant species growing in well drained soil	39.3232 / –86.4131	2001–2008	*Dragoni et al.* [2011]
U.S.-UMB	Michigan Biological Station	DBF	89-year-old Bigtooth Aspen, Quaking Aspen, Northern Red Oak and Hemlock with conifer understory	45.5598 / −84.7138	2001–2004 2006–2008	*Nave et al.* [2011]
U.S.-Los	Wisconsin Lost Creek	DBF	Minimum of 55-year-old Speckled Alder, Willow, bog Birch and Redosier Dogwood overstory with Sedge understory growing on poorly drained soil	46.0827 / −89.9792	2001–2006	*Sulman et al.* [2009]
U.S.-NE1	Nebraska Mead-irrigated continuous maize site	CL	Maize crop irrigated with a center pivot system	41.1651 / –96.4766	2002–2009	*Verma et al.* [2005]
U.S.-NE2	Nebraska Mead-irrigated maize-soybean rotation site	CL	Maize-soybean rotation irrigated with a center pivot system	41.1651 / –96.4766	2002–2009	*Verma et al.* [2005]
U.S.-NE3	Nebraska Mead-rainfed maize-soybean rotation site	CL	Rainfed maize-soybean rotation	41.1797 / −96.4396	2002–2009	*Verma et al.* [2005]

[a]ENF: evergreen needleleaf forest; DBF: deciduous broadleaf forest; CL: crop land.

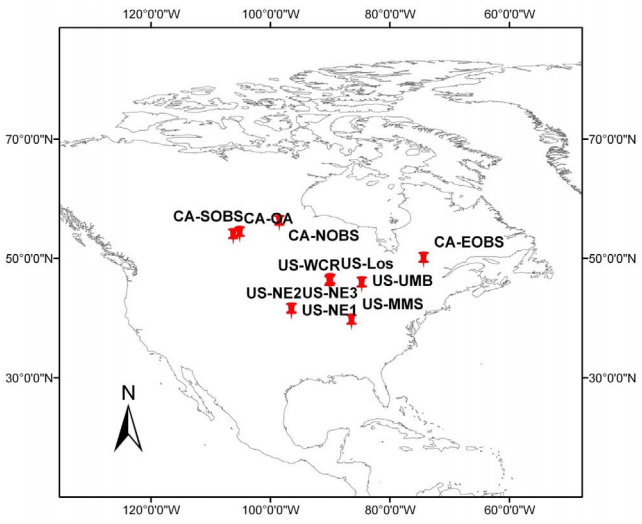

Figure 1. CO_2 flux tower sites across North America.

is 810–880 mm with rare to no snowfall. The agricultural sites represent various tillage system, crop rotation, and crop composition of typical North American croplands. NE1 and NE2 are irrigated whereas NE3 is rainfed (Table 1). The crop canopy height is less than 3 m. Agricultural residues are usually left on the site.

[11] We used 83 site-years of gross primary production (GPP) data available from the CCP and AmeriFlux networks measured using the eddy covariance (EC) technique. The EC technique is the state-of-art method for measuring ecosystem-level fluxes of carbon, which therefore match the LSP computation at a spatial scale comparable to satellite pixels. Wind velocity components (u, v, w, measured using 3-D sonic anemometers), air temperature, water vapor density, and CO_2 concentration were sampled at 10 to 20 Hz, and calculations of relevant covariances were performed from these samples to obtain the fluxes. A standard procedure was used to estimate the daily GPP from half-hourly values of net ecosystem exchange (NEE):

$$\mathrm{GPP} = \mathrm{NEP} + \mathrm{R}, \tag{1}$$

where NEP is the net ecosystem production (−NEE) and R is the ecosystem respiration. GPP (dag m^{-2} d^{-1}) was estimated from equation (1) or zero (nighttime and during periods when both soil and air temperature were less than 0°C. For CCP sites, a standard procedure was used to estimate the daily gross primary productivity (GPP) from gap-filled half-hourly measurements of NEE [*Barr et al.*, 2004]. Empirical regressions of nighttime NEE to temperature and daytime GPP to photosynthetically active radiation (PAR) were used to estimate GPP to fill gaps [*Barr et al.*, 2004]. For the AmeriFlux sites, level-4 daily products were used which contain gap-filled and friction velocity, u* filtered records of carbon fluxes using the Marginal Distribution Sampling (MDS) method [*Reichstein et al.*, 2005]. Although different gap-filling methods were used among CCP and AmeriFlux data sets, most partitioning methods were found to yield similar seasonal cycles [*Richardson et al.*, 2012]. We assume that the large part of the CO_2 flux measurements contributing to seasonal LSP phase changes comes from the 500 m × 500 m footprint area of the flux tower, equivalent to the MODIS pixel size used for LSP DOY extraction. Ninety percent of stable (day time) CO_2 flux, used for GPP, usually comes from the area less than 500 m of the tower site [*Chen et al.*, 2009].

3. Methods

3.1. Phenology Index From Optical Satellite Measurements

[12] Methodologies to estimate LSP from optical satellite remote sensing center on various uses of NDVI time series. NDVI is calculated from red and NIR reflectances as follows:

$$\mathrm{NDVI} = \frac{(\mathrm{NIR} - \mathrm{red})}{(\mathrm{NIR} + \mathrm{red})}. \tag{2}$$

[13] Critically speaking, in addition to radiation absorption by vegetation canopies, NDVI includes aggregate, confounding influence of atmospheric contamination, cloud cover, snow cover, and soil reflectance. *Shabanov et al.* [2002] have analyzed the time evolution of red and NIR reflectances in northern Europe during spring months from 1981 to 1994, and concluded that the trend observed from NDVI is not only related to SOS but also to a reduction in the snow cover extent, which agrees with observations made by *Dye and Tucker* [2003]. In northern temperate and boreal forests (Figure 2: CA-OA, U.S.-Los, U.S.-UBM, U.S.-WCR), the delayed period (shoulder) between the snowmelt and the SOS, and EOS and snowfall indicated by the negative NDII and positive NDVI complicates the determination of the exact date of SOS, and EOS by use of NDVI. NDVI increases during both snowmelt and leaf appearance, resulting in either one continuous increase, or in two distinct increases if snowmelt ends before the leaf appearance (Figure 2) [*Delbart et al.*, 2005]. Close examination of the spectral reflectance curves (Figure 3) indicates that the NDVI shoulder for the time when NDII is below 0 corresponds to soil background or vegetation state before greening – for example reflectances of barks and dry understory. The trends are the same in the autumn season. The NDVI value for the 3 soil types in Figure 3 is 0.1–0.4, whereas the dry vegetation has NDVI value of 0.2 for the MODIS bands (spectral response functions) while both dry vegetation and the 3 soils resulted in NDII < 0. To help discriminate the effects of vegetation phenology from background phenomena such as accumulation and melting of snow, researchers have begun to examine alternative vegetation indices [*de Beurs and Henebry*, 2008, 2010; *Delbart et al.*, 2005; *Delbart et al.*, 2006; *Delbart et al.*, 2008]. These researchers argue that the use of NDVI in boreal broadleaf forests suffers from uncertainty in predicting SOS due to the effects of snow cover and snowmelt. They further suggest the use of the normalized difference infrared index (NDII) [*Hardisky et al.*, 1983], which is based on the NIR and SWIR reflectances, to reduce these uncertainties. The NDII is calculated as:

$$\mathrm{NDII} = \frac{(\mathrm{NIR} - \mathrm{SWIR})}{(\mathrm{NIR} + \mathrm{SWIR})}. \tag{3}$$

[14] In northern latitudes where snowmelt may trigger an increase in NDVI prior to SOS, NDII proves useful for

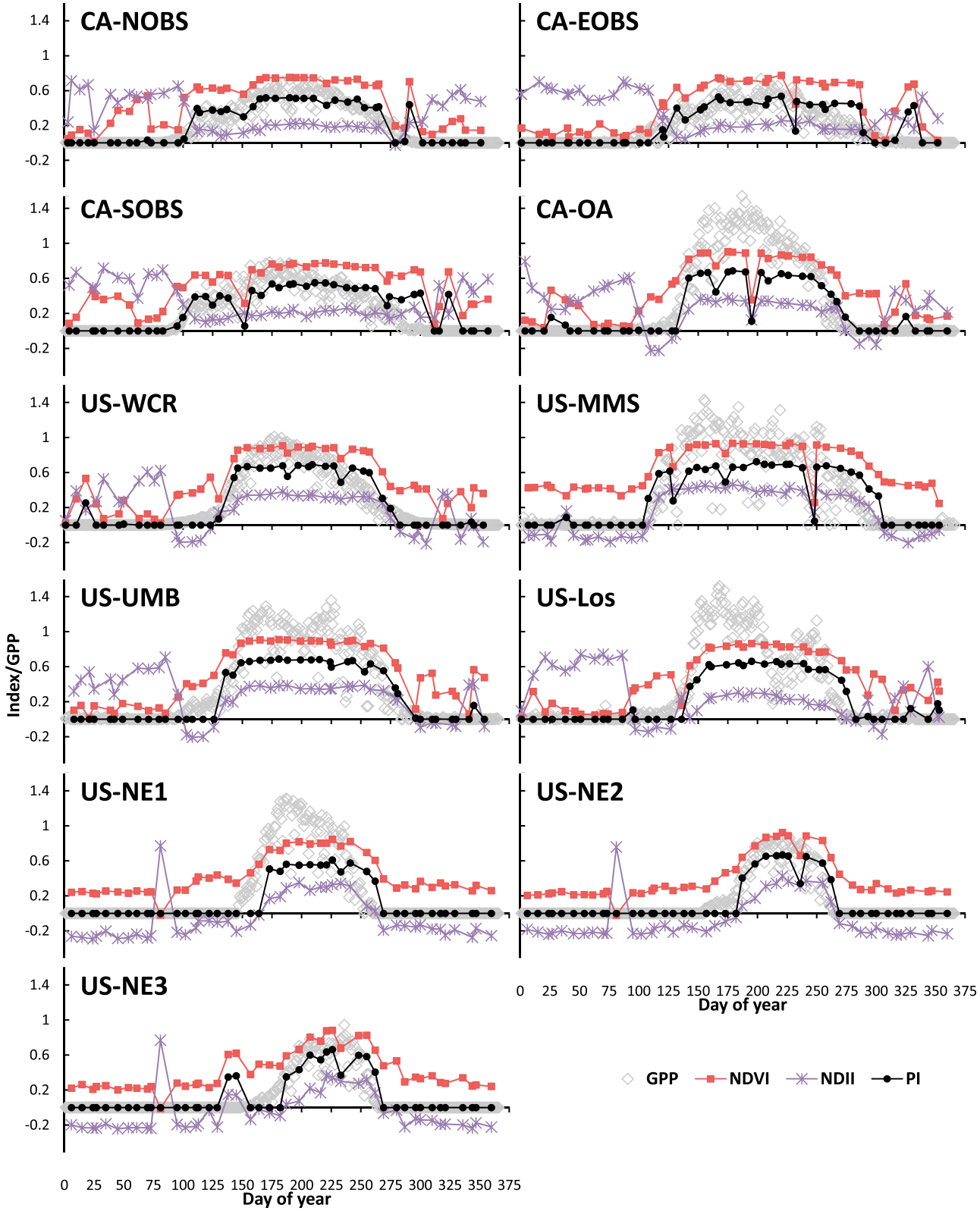

Figure 2. Example time evolution of normalized difference vegetation index (NDVI), normalized difference infrared index (NDII), phenology index (PI), and gross primary production (GPP) for all 11 CO_2 flux tower sites for common measurement year 2006. Open squares are GPP, solid squares are NDVI, asterisks are NDII, and solid circles are PI.

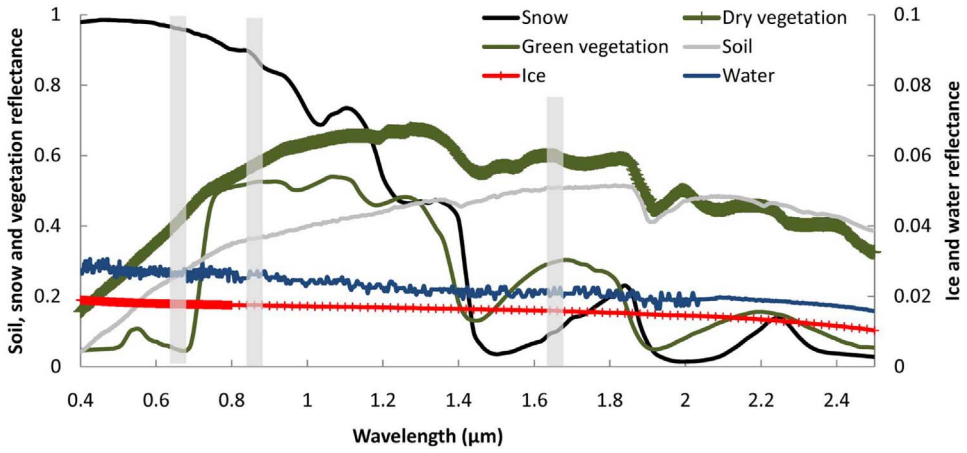

Figure 3. Spectral reflectance curve of major land surface cover types from Aster Spectral Library [*Baldridge et al.*, 2009]. The green vegetation spectrum is an average from three spectra, each representing conifer, deciduous and grass reflectances. Soil spectrum is an average from three spectra, each representing light yellowish brown loamy sand, pale brown silty loam and dark reddish brown organic-rich silty loam. The snow spectrum is an average of three spectra representing coarse, medium and fine granular snow. The vertical gray bars show the location of MODIS red, near-infrared and shortwave-infrared spectral bands.

eliminating snowmelt versus vegetation growth confusion in broadleaf forests (e.g., Figure 2: CA-OA site, U.S.-Los, U.S.-UBM, U.S.-WCR). Snowmelt can be seen as a decrease in NDII values and subsequent vegetation green-up results in an increase in values. The main drawback of NDII is that when vegetation green-up occurs during snowmelt, typical of boreal needleleaf forest, the NDII decrease can mask the increase due to green-up (Figure 2: CA-NOBS, CA-SOBS, CA-EOBS). In addition to this, NDII alone cannot capture SOS and EOS, since it responds to land surface moisture both from the landscape and vegetation components. In temperate broadleaf forests and croplands, NDVI or NDII alone is also contaminated by seasonal dynamics of soil moisture and snow confounding LSP cycles (Figure 2).

[15] Combining the merits of NDVI and NDII thus may allow the subtle transition dates of SOS and EOS to be captured, as both indices compensate their respective drawbacks. Here, we propose a new index called the phenology index (PI) derived from the combination of NDVI and NDII as follows:

$$\mathrm{PI} = \begin{cases} 0, \text{if NDVI or NDII} < 0 \\ (\mathrm{NDVI} + \mathrm{NDII})^{*}(\mathrm{NDVI} - \mathrm{NDII}) = \mathrm{NDVI}^2 - \mathrm{NDII}^2 \\ 0, \text{if PI} < 0 \end{cases} \tag{4}$$

[16] PI derived as a product of the sum and difference of NDVI and NDII appears to be a good indicator of SOS and EOS, as can be seen in Figure 2, largely following the GPP time series with smooth temporal curve compared to NDVI or NDII throughout the year. Vegetation indices (VIs) are usually constructed in simple arithmetic transformations of two or more spectral bands in a way that the VI should correlate with a variable which is difficult to measure directly and are often constructed for a single purpose. The purposes can be generally categorized as "brightness", "greenness" and "wetness" [*Coppin and Bauer*, 1994]. VIs are not intrinsic physical quantities, and several studies have attempted to empirically modify the existing VIs to remove the confounding effect of brightness (mainly soil) and wetness (mainly from land surface moisture) from greenness that responds to the development of photosynthetic biomass [e.g., *Brown et al.*, 2000; *Gonsamo*, 2011; *Gonsamo and Pellikka*, 2012; *Huete et al.*, 1997]. Figure 2 shows that both NDVI and NDII respond not only to the development of photosynthetic biomass (greenness) but also to soil exposure (brightness); and snow, soil and land surface moisture (wetness) suggesting that NDVI or NDII alone cannot remove the confounding effect of brightness and wetness on LSP time series. Other major observation from Figure 2 is that NDVI and NDII have opposing trends with increasing brightness and wetness, and similar trends with increasing greenness. Therefore, we have empirically constructed PI in order to remove the wetness and brighten effect on greenness. PI is constructed on the basis of the following rationale: (1) NIR reflectance is less than red reflectance for ice, snow and water (Figure 3) resulting in NDVI < 0 for which PI becomes 0; (2) SWIR reflectance is less than NIR for soil and for non photosynthetic vegetation component resulting in NDII < 0 and NDVI > 0 for which PI becomes 0 (Figure 3); (3) if NDII > NDVI, the green vegetation or land surface is covered by snow for which PI becomes 0 (Figure 3); (4) the use of PI instead of NDVI or NDII masks out the time series of permanently non vegetated landscape for which NDVI or NDII may result in spurious time series due to moisture variations resembling vegetation LSP; and (5) the product of the sum and the difference of NDVI and NDII gives a pronounced and smooth curve, removes the effect of wetness from the greenness, and avoids the local solution if we simply consider the use of NDVI once the above criteria (1, 2, 3 and 4) are met, which may particularly occur in boreal forests due to intermittent loading and unloading of snow (Figure 2: CA-NOBS, CA-SOBS, CA-EOBS, CA-OA). One could argue that a more elegant mathematical formulation of PI would directly use the red, NIR and SWIR bands, but our attempts suggest that there is no simple solution to simultaneously remove brightness and wetness effects from greenness trends. PI is actually the

squared greenness minus squared wetness in the growing season.

[17] We have used a zero PI value for the non-vegetated part of time series which is in accordance with the standard MODIS and AVHRR VI products. PI captures both SOS and EOS in needleleaf forest, broadleaf forest and agricultural crops, whether there is an overlap between SOS and snowmelt (Figure 2: CA-NOBS, CA-SOBS, CA-EOBS), a lack of overlap characterized by the persistent shoulder of NDVI and the negative values of NDII because of the exposed soil (Figure 2: CA-OA, U.S.-WCR, U.S.-Los, U.S.-UBM), or where there is no prevalent snow cover (Figure 2: U.S.-MMS, U.S.-NE1, U.S.-NE2, U.S.-NE3). PI uses more spectral information than either of NDVI or NDII alone, while the use of SWIR also reduces aerosol interferences in surface reflectance. PI has relatively steeper slopes for the SOS and EOS transition dates. There will still be some remnants of contaminated pixels due to missing or poor quality satellite data, although PI has smoother curves than NDVI and NDII. For this, we can easily implement an automated SOS and EOS determination algorithm with an appropriate data filtering technique.

3.2. Deriving Phenology Metrics From Vegetation Indices and GPP

[18] Several methodologies [*Fisher et al.*, 2006; *Schwartz and Hanes*, 2010; *White et al.*, 2009] used to assess SOS and EOS from NDVI and other remote-sensing-based VIs have been presented in literature. There is a strong need to characterize interannual variability of SOS and EOS with a functional representation that is objective, consistent and stable among years and different land cover types. In this study, we focus on the modified use of the double logistic function:

$$y(t) = \alpha_1 + \frac{\alpha_2}{1 + e^{-\partial_1 (t-\beta_1)}} - \frac{\alpha_3}{1 + e^{-\partial_2 (t-\beta_2)}}, \qquad (5)$$

where $y(t)$ is the observed NDVI, PI or GPP at day of year (DOY) t, and α_1 is the background NDVI, PI, or GPP. The formula $\alpha_2 - \alpha_1$ represents the difference between the background and the amplitude of the spring and early summer plateau, and $\alpha_3 - \alpha_1$ represents the difference between the background and the amplitude of the late summer and autumn plateau both in NDVI, PI or GPP units. The parameters ∂_1 and ∂_2 are the transitions curvature parameters (normalized slope coefficients), and β_1 and β_2 are the midpoints in DOYs of these transitions for green-up and senescence/abscission, respectively (details in Figure 4). In contrast to [*Fisher et al.*, 2006] we use different amplitudes during the first and second halves of the growing seasons with the intention that the ascendant (green-up) and descendent (senescent) parts can differ both in shape and in maximum values (Figure 4). A schematic of the curve structure fit to the MODIS PI and flux GPP values is shown in Figure 4. The smooth fit lines of PI in Figures 4a and 4b show that the use of 7 rather than 6 parameters helps to capture the quick rise of PI. During the iterative curve-fitting of equation (5), we further used weights to reduce the impacts of poor quality PI and NDVI data points. We have developed a simple weighting scheme, which gives a weight of half for the sum-of-squared-error for the value of PI or NDVI of the central point if they are less than half or more than twice the median value of the moving window average of three points in the iterative curve-fitting process. This will not affect the ascending and descending inflection points – as these always are the median values. The points before and after the inflection points also fall as a median value in their respective moving window. We believe that the three point window of 8-day values of indices is adequate to reduce the effect of poor quality data on the curve-fitting. Data were fitted to the logistic function with a nonlinear regression provided with the first guess values of the seven parameters in equation (5), and solved with maximum of 2000 iterations.

[19] While the midpoint DOYs (β_1 and β_2) are good indicators of SOS and EOS from an NDVI time series, these midpoints will not capture the SOS and EOS from PI and GPP time series (Figure 2 and Figure 4). For GPP and PI, SOS is the start of the slope of the ascending curve and EOS is the end of descending curve (Figure 4) since PI appears to follow that of land surface photosynthesis (GPP). Throughout this paper, SOS and EOS determined by start and end of the spring and autumn slope points, respectively, are used for PI and GPP (Figure 4). For NDVI, we use only midpoint SOS and EOS DOYs. The start and end DOYs of both slopes can be calculated as $f(\alpha_1, \partial_1, \beta_1)$ for SOS and $f(\alpha_2, \partial_2, \beta_2)$ for EOS. Since there will be rigorous mathematical steps involved in deriving the start and end of the curvatures from the third derivative of equation (5), we here demonstrate the final steps for practical use. Mathematically, the average slopes "during the transitions" DOYs between the background and the amplitude ranges in equation (5) are the product of these ranges and the slopes, i.e., $\alpha_2\partial_1/4.562$ and $\alpha_3\partial_2/4.562$ for ascendant and descendent parts, respectively. Given the average slopes, α, ∂ and β values, the final results for both PI and GPP can be calculated as:

$$\mathrm{SOS} = \beta_1 - 4.562/(2\partial_1) \qquad (6)$$

$$\mathrm{EOS} = \beta_2 + 4.562/(2\partial_2). \qquad (7)$$

3.3. Statistical Analysis

[20] Since the LSP estimates from CO_2 flux measurements and remote sensing observations are not without error, we apply robust regression and correlation approaches. For analysis of the relationships among the LSP estimates from GPP, NDVI, and PI, we use Spearman's correlation coefficient and type II regression (i.e., geometric mean regression). When we explore the relationship between variable y and x, for example, we first regress y on x and obtain a slope (β_{yx}). Second, we regress x on y to obtain the inverse slope (β_{xy}). The final slope between y and x for this type II regression was calculated as:

$$\beta = [\mathrm{sign}(R)]\sqrt{\frac{\beta_{yx}}{\beta xy}}, \qquad (8)$$

where [sign(R)] is the sign (+/−) of the correlation coefficient. With this new slope, we can then calculate the new intercept (α) as:

$$\alpha = \hat{y} - \beta\hat{x}, \qquad (9)$$

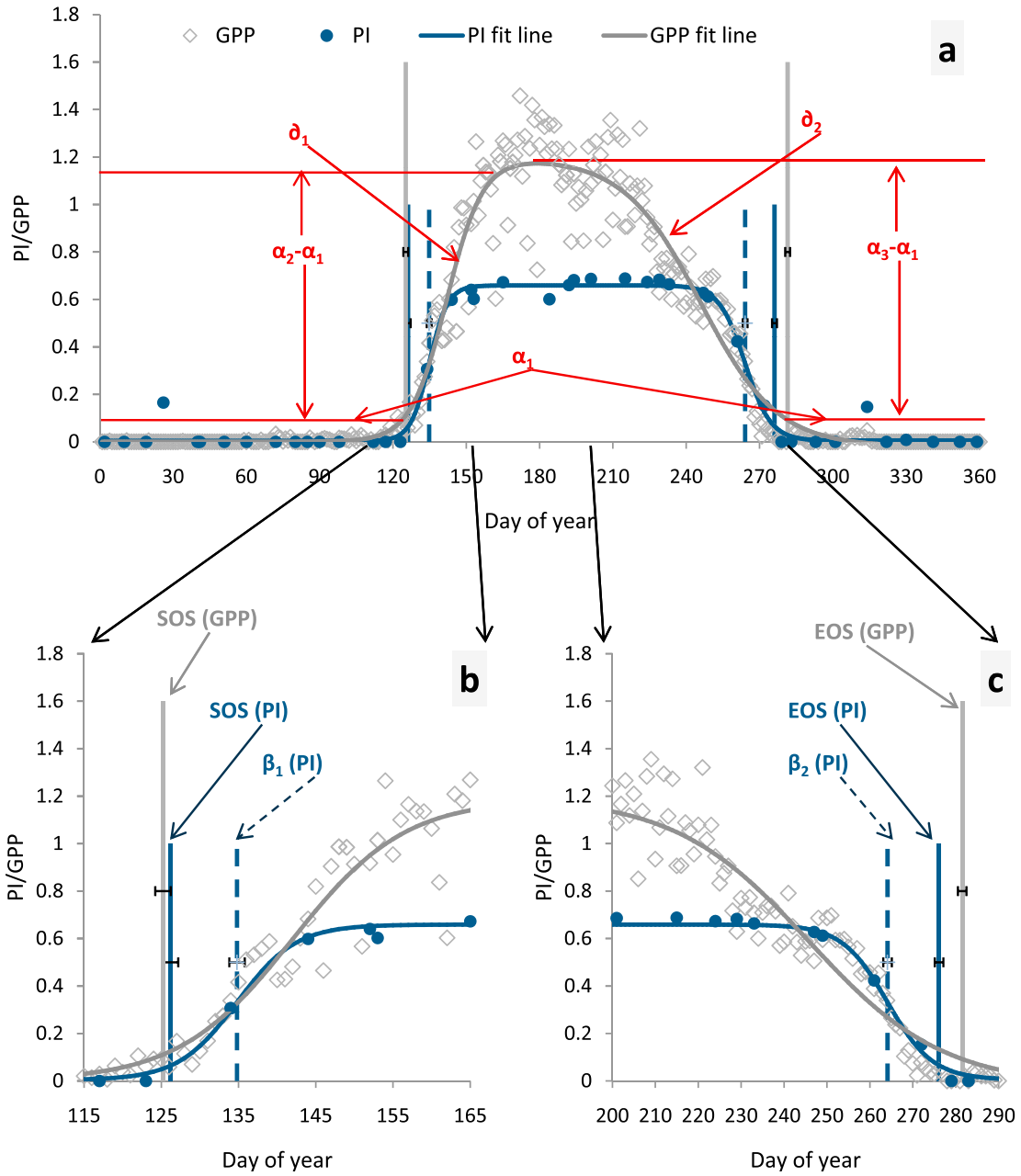

Figure 4. (a) Schematic of curve-fitting mechanism for PI and daily GPP (dag m^{-2} d^{-1}) time series for the Saskatchewan Old Aspen flux tower pixel for year 2001. PI data points that fall further from the fit line are subsequently assigned less weight in the phenological fit. Both the PI (solid circles) and GPP (open diamonds) were fitted using a double logistic function. (b–c) Zooms into the ascendant (green-up) and descendent (senescent) parts of Figure 4a. All parameters of equation (5) are illustrated.

where $\hat{y}$ and $\hat{x}$ are mean values of y and x, respectively. All regression and correlation analyses are reported as above unless stated otherwise.

4. Results

4.1. Visual Evaluation of the New Phenology Index

[21] First, we start with visual inspection of PI, in comparison with NDVI and NDII time series interpreted with the aid of our understanding of spectral signature of land surface components (Figure 3) and temporal evolution of land surface photosynthesis (i.e., GPP). We have shown in Figure 2 that the ENF, DBF, and CL sites have contrasting NDVI and NDII annual cycles for changes in wetness and brightness, with distinct signatures of winter snow cover, background soil, snowmelt, spring green-up, summer plateau and autumn senescence. At the ENF sites (Figure 2: CA-NOBS, CA-EOBS, CA-SOBS), the high variability of the NDVI during the snow covered period resulted from the intermittent loading and unloading of intercepted snow on the forest canopy. In the DBF site where there is no prevalent snowfall in winter (Figure 2: U.S.-MMS), and in all the

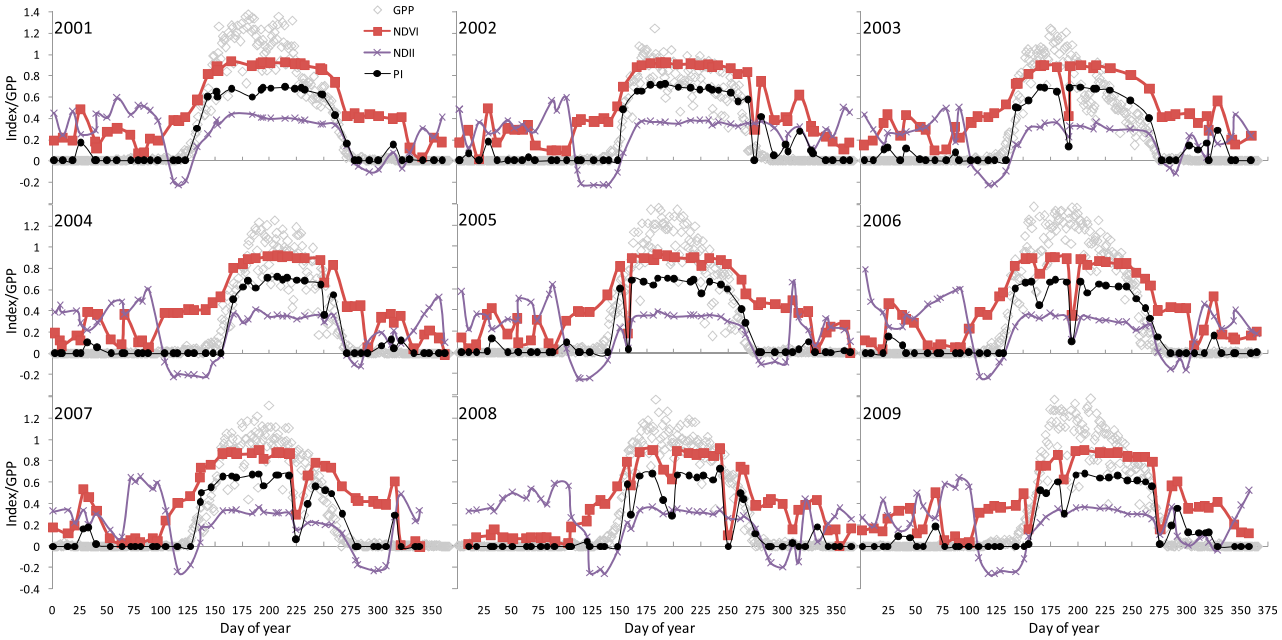

Figure 5. Example time evolution of normalized difference vegetation index (NDVI), normalized difference infrared index (NDII), phenology index (PI), and gross primary production (GPP) for Old Aspen (OA) flux tower site for years 2001–2009. Open diamonds are GPP, solid squares are NDVI, x's are NDII, and solid circles are PI.

three CL sites (Figure 2: U.S.-NE1, U.S.-NE2, U.S.-NE3), both NDVI and NDII show smoother curves compared to the other sites. In the DBF sites where there is prevalent snowfall for most of the winter (Figure 2: CA-OA, U.S.-WCR, U.S.-UMB, U.S.-Los), there are two distinct gradients of NDVI and NDII before SOS. The same is also true after EOS. The seasonal cycle of NDVI or NDII has different phenological significance for the ENF, DBF, and CL sites, indicating the difficulties for phenology studies if NDVI is not coupled with NDII where the land cover type is unknown. NDVI and NDII both respond to the appearance and disappearance of snow, exposure of soil or non photosynthetic plant components, and the optical thickness of the photosynthetic biomass (greenness). At the ENF sites (Figure 2: CA-BOBS, CA-EOBS, CA-SOBS), interpretation with the GPP curve shows that SOS occurs during the spring canopy thaw, i.e., it coincides with snowmelt resulting in increased NDVI and masking the response of NDII, whereas EOS occurs during the autumn freeze, which may or may not be accompanied by snow accumulation and persistent freezing temperatures. We know that during the spring and autumn shoulders of NDVI, NDII values become negative indicating the landscape is bare from photosynthetic biomass. Therefore, the increase of NDII in spring after snowmelt is due to vegetation growth, which can be cross inspected with increasing NDVI if it is otherwise due to rainfall and vice versa for the autumn (Figure 2). These two points, which we call the SOS and EOS, are rather consistently captured using PI across the three plant functional types (Figure 2 and Figure 5). The close examination of Figure 2 indicates three things: (1) PI follows consistently the GPP curve compared to NDVI or NDII across the three plant functional types, (2) EOS which has been illusive to capture using remote sensing data has shown to be measurable using PI although NDII also performs well at DBF and CL sites, and (3) the start of PI increase comes 2 weeks later for some of the DBF and CL sites compared to the time GPP starts increasing. The explanation for the latter is that photosynthesis may start earlier than the accumulation of photosynthetic biomass which can be measured by satellite optical sensors.

[22] Figure 5 presents the time dynamics of NDVI, NDII, PI, and GPP for the CA-OA flux tower site for years 2001–2009. Three main points can be noted from these results. First, although NDVI tends to follow the time dynamics of the vegetation LSP indicated by the GPP time series, the start and end of measurable photosynthesis cannot be captured and varies interannually. Second, NDII follows the vegetation LSP once snow has melted and the soil surface becomes dry. Although NDII can substantially capture both SOS and EOS, this is not true for needleleaf sites as indicated in Figure 2. The water contained in live vegetation in early spring and late autumn masks the trend of NDII in needleleaf forests (Figure 2). Third and most important, the PI, having the merits of both NDVI and NDII, follows the time dynamics of GPP more closely and thus tracks vegetation LSP (Figure 4). As also noted by [*Delbart et al.*, 2005], NDII may prove useful for DBF and CL sites, however the implementation of objective functions to extract SOS and EOS is challenging. Therefore, we have not considered the SOS and EOS dates extracted from NDII in the current comparison.

4.2. Intercomparison of SOS and EOS as Retrieved From NDVI, PI and GPP

[23] One of our objectives was to compare SOS and EOS as estimated from CO_2 flux data and remote sensing observations. Figure 6 presents the SOS and EOS intercomparisons

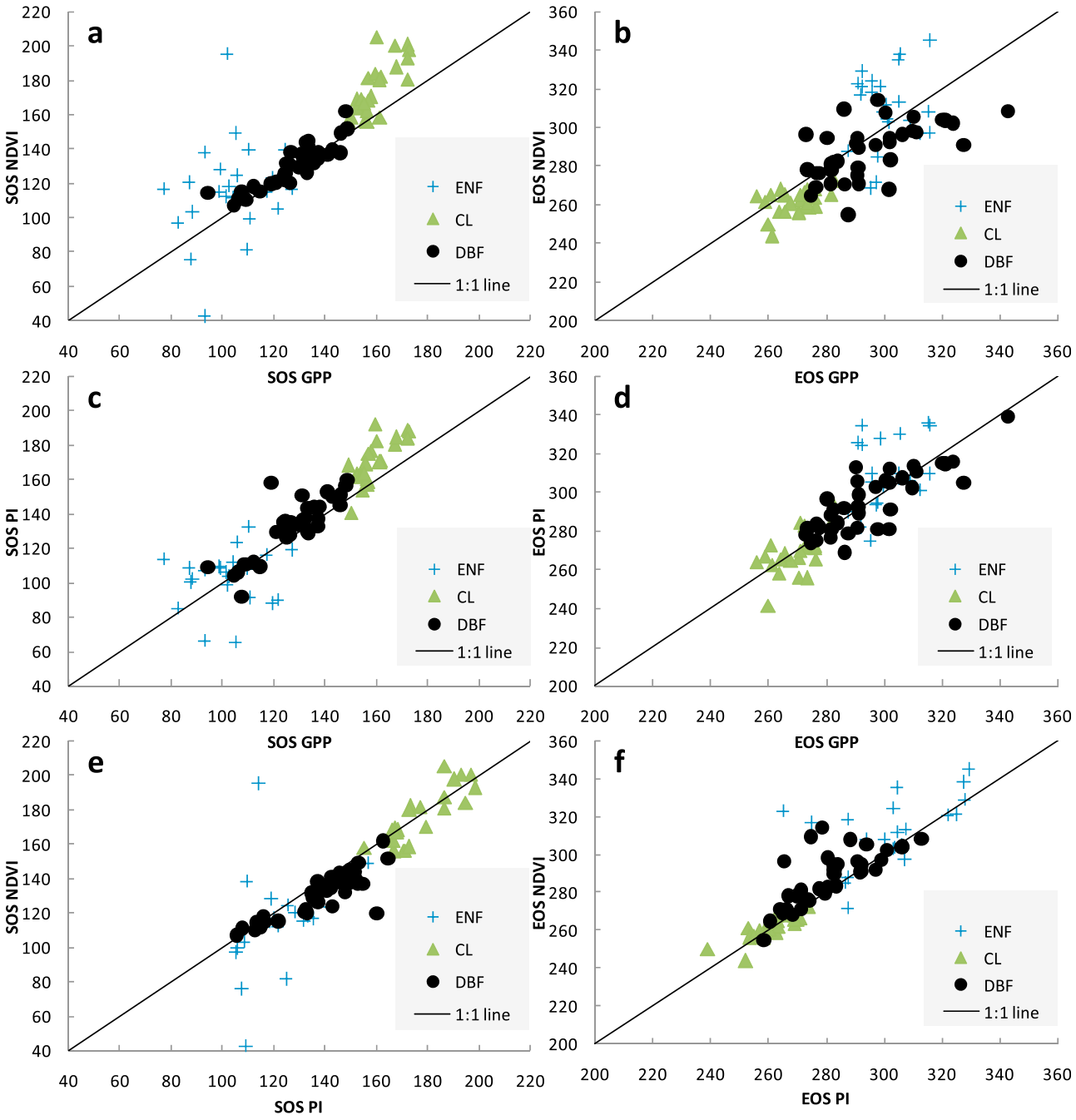

Figure 6. Scatterplots of start of season (SOS) and end of season (EOS) dates as estimated from normalized difference vegetation index (NDVI), phenology index (PI), and gross primary production (GPP) for the three plant functional types: evergreen needleleaf forest (ENF), indicated by crosses; deciduous broadleaf forest (DBF), indicated by solid circles; and cropland (CL), indicated by solid triangles.

among NDVI, PI and GPP methods, and Table 2 presents the associated measures of agreement. The overall results indicate that SOS and EOS from PI are more comparable to GPP (reduced RMSE and bias, and higher correlation) than NDVI is to GPP (Figure 7). One of the intriguing results is that both SOS and EOS estimates differences between NDVI and GPP are statistically correlated with the difference between NDVI- and PI-based estimates (Figure 8). This indirectly indicates that the within site interannual SOS and EOS estimates trends from PI are more comparable to GPP SOS and EOS estimates than NDVI is to GPP estimates (Figure 9). Forty-two percent of growing season length estimated from PI is within 8 days' difference, equivalent to the satellite data temporal resolution, compared to GPP-based estimates, whereas only 15% of NDVI-based estimates fall in that range (Figure 9). The other major finding of this study is that EOS both from PI and NDVI is more comparable to GPP EOS estimates than SOS estimates among the three methods. This proved that EOS is measurable

Table 2. Quantitative Measures of the Agreement Between the SOS and EOS Dates Retrieved Using the NDVI, PI, and GPP Methods: Spearman's Correlation Coefficient (R), Root Mean Square Error (RMSE), and Type II Regression (i.e., Geometric Mean Regression) Intercept (α) and Slope (β)[a]

		NDVI = α + βGPP				PI = α + βGPP				NDVI = α + βPI			
		ENF	DBF	CL	All	ENF	DBF	CL	All	ENF	DBF	CL	All
SOS	α	−104.77	5.75	−169.02	−22.86	−28.09	−27.76	−114.20	−23.99	−57.66	27.36	−31.07	1.54
	β	2.14	0.97	2.16	1.25	1.28	1.25	1.79	1.23	1.68	0.78	1.21	1.02
	RMSE	28.95	5.94	10.40	17.82	17.20	9.06	8.40	12.93	28.70	6.73	8.49	17.65
	R	0.24	**0.88**	**0.74**	**0.84**	0.24	**0.78**	**0.79**	**0.92**	0.32	**0.70**	**0.81**	**0.83**
	Bias	−12.89	−2.49	−15.76	−9.13	−0.43	−4.46	−11.27	−5.30	10.46	8.36	1.09	6.86
EOS	α	−401.13	33.76	23.30	−87.24	−297.34	17.59	−140.82	−53.53	44.95	17.66	105.17	−29.28
	β	2.36	0.86	0.88	1.29	2.02	0.94	1.52	1.19	0.85	0.92	0.58	1.08
	RMSE	19.99	11.98	5.84	16.56	16.25	9.28	8.91	12.32	16.43	9.81	3.62	11.94
	R	0.02	**0.57**	0.38	**0.77**	0.34	**0.76**	**0.57**	**0.85**	**0.67**	**0.73**	**0.64**	**0.87**
	Bias	−9.02	7.94	8.01	3.31	−8.49	0.62	0.72	−1.84	−9.02	−6.08	−0.23	−5.21

[a]Bold type indicates that correlation is significant at the 0.05 p-value level (2-tailed). ENF (n = 23), DBF (n = 37), and CL (n = 24). ENF: evergreen needleleaf forest; DBF: deciduous broadleaf forest; CL: crop land.

using remote sensing observations, which was not fully evident from the large number of past studies dedicated to spring phenology.

[24] There are distinct patterns of LSP agreement among ENF, DBF and CL sites. The negative bias of SOS from PI and NDVI compared to GPP estimates for DBF and CL indicates that both remote-sensing-based methods overestimate SOS. There was no statistically significant correlation among GPP-, PI- and NDVI-based SOS estimates for ENF sites whereas the only significant correlation for EOS estimate for ENF sites was between PI and NDVI estimates (Figure 6, Table 2). However, reduced RMSE, dispersion and bias between PI and GPP SOS and EOS estimates compared to NDVI and GPP estimates show that PI gives slightly improved estimate. A close examination of Figure 2, Figure 6 and Table 2 statistics shows that neither NDVI nor NDII are reliable indicators of phenology in boreal needleleaf forests. These findings are also strongly supported by other studies [*de Beurs and Henebry*, 2010; *Delbart et al.*, 2006; *Delbart et al.*, 2008; *Peckham et al.*, 2008; *White et al.*, 2009]. Since most boreal forests in North America are dominated by needleleaf tree species, the use of NDVI over this large area raises significant concerns. One should note that, although MODIS data are 8-day composites, there are several points where the exact difference of two consecutive dates' retrieval exceeded 8 days (Figure 2 and Figure 4). More estimates from PI fall within 8 days' difference than NDVI compared to GPP-based estimates for ENF sites, i.e., 13%(39%), 26%(48%), and 0%(31%) for SOS, EOS and growing season length, respectively, when GPP estimates are compared with NDVI (PI).

5. Discussion

[25] Several studies have reported contrasting findings of phenology and NDVI trends in Northern latitudes [*White et al.*, 2009]. Therefore, an unsettling debate is emerging about the use of NDVI as LSP indictor and its ability to

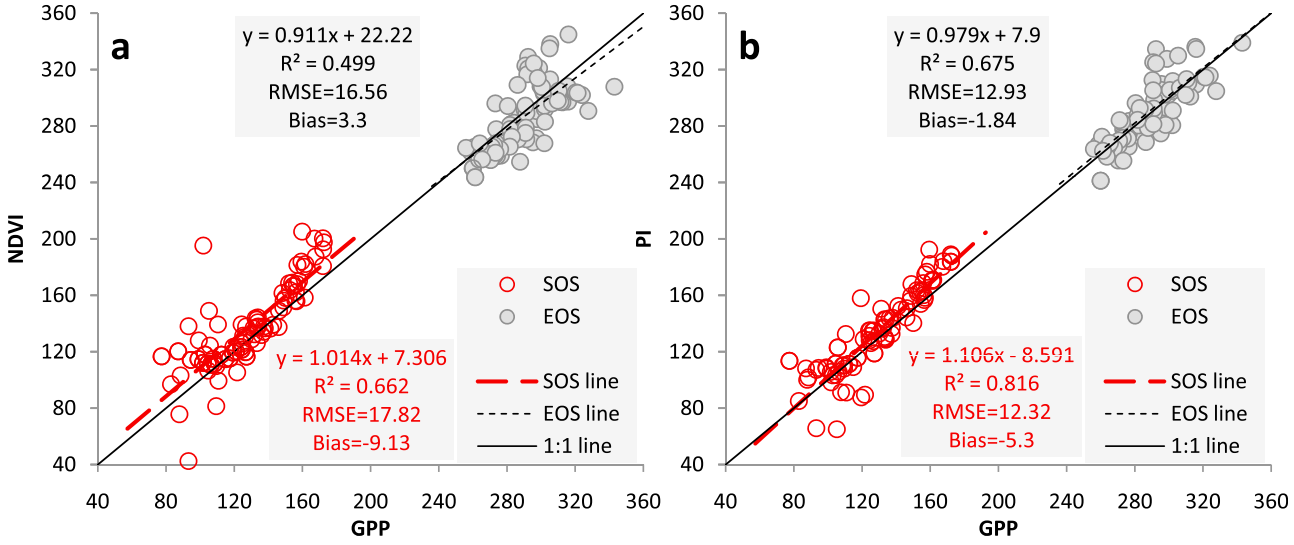

Figure 7. Scatterplots of start of season (SOS) and end of season (EOS) dates as estimated from normalized difference vegetation index (NDVI), phenology index (PI), and gross primary production (GPP). Solid circles are EOS, and open circles are SOS. Statistics for ordinary least squares (OLS) regression and coefficient of determination are also given.

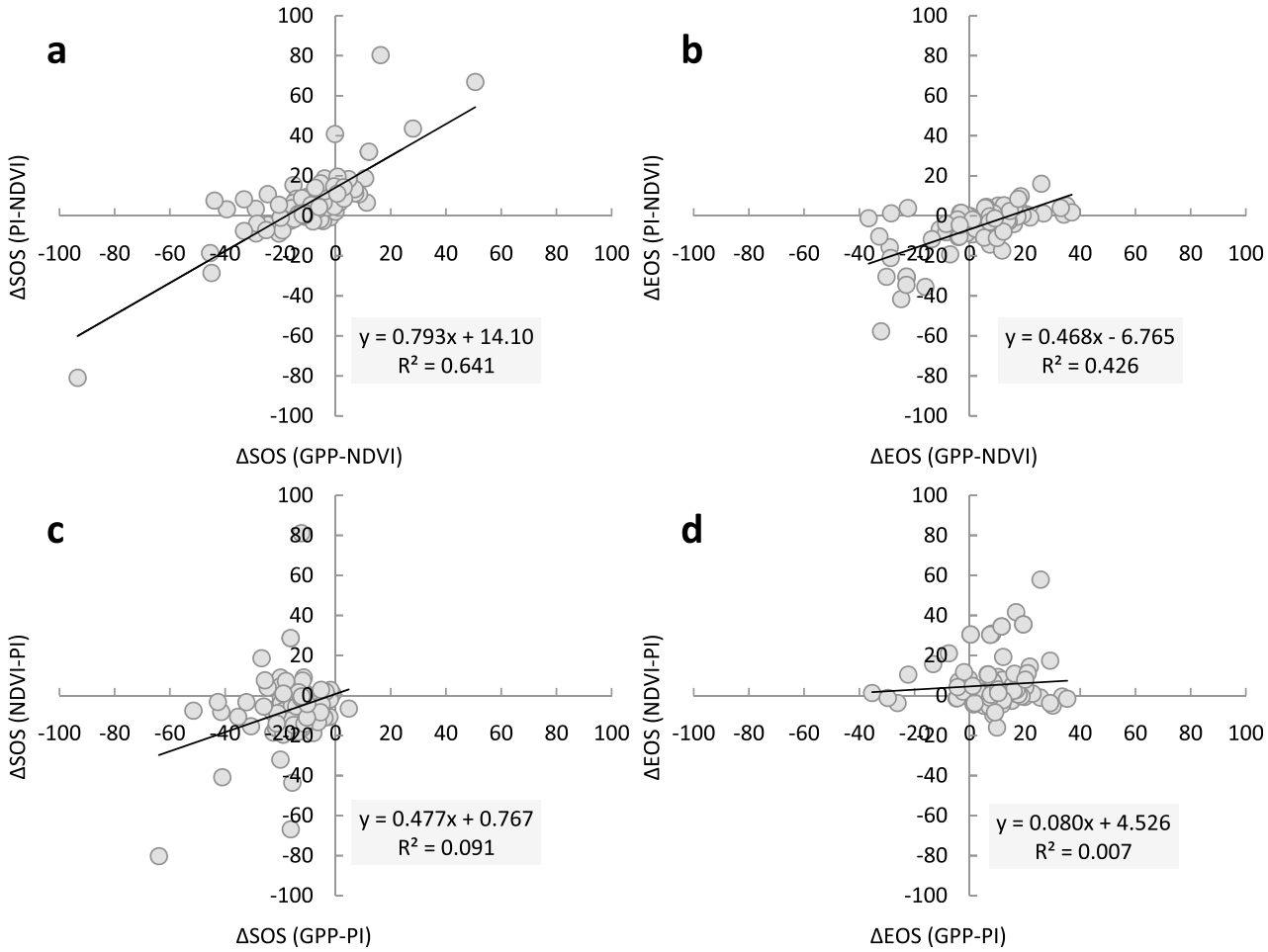

Figure 8. Scatterplots of start of season (SOS) and end of season (EOS) differences as estimated from normalized difference vegetation index (NDVI), phenology index (PI), and gross primary production (GPP). Correlation is significant at the 0.05 *p*-value level (2-tailed) for Figures 8a and 8b. Statistics for ordinary least squares (OLS) regression and coefficient of determination are also given.

capture SOS and EOS for a wide range of vegetation and land surface conditions [*Alcaraz-Segura et al.*, 2010; *White et al.*, 2009]. These difficulties raise concerns about whether the observed LSP trends are artifacts of the data or methodologies used to extract SOS and EOS. These questions remain to be answered with robust methodologies for the assessment of the LSP metrics.

[26] In this study, we have extended the methodologies of LSP extraction from optical satellite data and CO_2 flux measurements to improve estimates of SOS and EOS in temperate and boreal regions. The major aim was to compare CO_2 flux-based estimates of LSP dates with remote sensing estimates in three plant functional types. Most of the earlier studies are centered on the use of NDVI for LSP studies. However, recent exhaustive North American analysis of NDVI compared 10 different NDVI-based methods to extract SOS and found that individual methods differed in average day-of-year estimates by $\pm$60 days and in standard deviation by $\pm$20 days, compared with the ensemble average of all methods [*White et al.*, 2009]. This suggests that NDVI alone simply cannot capture the subtle changes in LSP. Therefore, we attempted to improve the LSP extraction from optical remote sensing aiming at decoupling the response of wetness and brightness in vegetation temporal dynamics in satellite measurements. Our study suggests that, in boreal needleleaf forest, remote-sensing-based LSP estimation is poor when compared with land surface photosynthesis-based LSP estimates, although PI gave slightly better results (Figure 9). There is no established definition of LSP in boreal needleleaf forest which makes the direct comparison of increase in green-up from remote sensing to increase in GPP challenging. Regardless of the comparison, if one carefully examines the SOS and EOS results (Figure 6, Figure 7, Figure 8, Figure 9 and Table 2), the overall results of PI are relatively better in the approximations of GPP estimates compared to NDVI.

[27] Most of the earlier LSP studies focus on SOS rather than EOS because the latter is difficult to estimate due to the slow process of vegetation browning and leaf abscission. Unlike previous studies, however, we use an objective measure to compare EOS estimates with the end of measurable photosynthesis in the flux tower sites for 3 plant functional types. Intriguingly, all of the remote-sensing-based methods show good performance in EOS estimation compared to GPP, even better compared to the relationship between SOS estimates from GPP and remote sensing. This

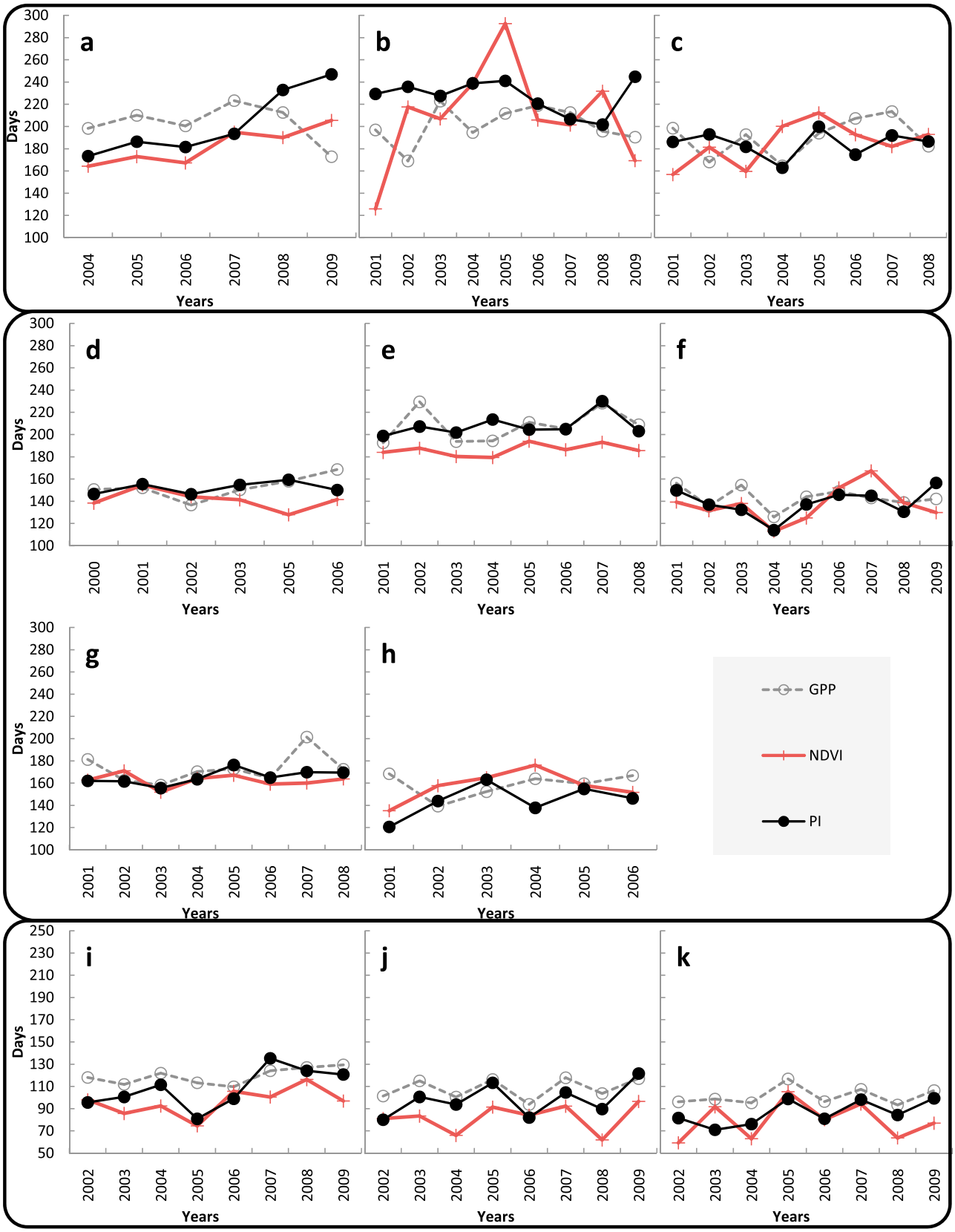

Figure 9

implies that EOS is actually a measurable phenological phenomenon. This encouraging result will extend the study of LSP and its implication on ecosystem productivity to autumn months. Extended and warming autumn is becoming an important factor of ecosystem carbon budget often resulting in higher ecosystem respiration and net carbon loss [*Piao et al.*, 2007; *Piao et al.*, 2008].

[28] *Delbart et al.* [2006] and *Delbart et al.* [2005] used NDII or a related index (normalized difference water index) with the underlying assumption that the NDII first decreases with snowmelt and then increases during initial vegetation growth (Figure 2). This approach has shown to capture the SOS and EOS in deciduous forests with snowy conditions in Siberia and has been found to be improvement over other methods [*Delbart et al.*, 2005, 2006]. This is also confirmed in this study as NDII shows the same trend as PI and photosynthesis, i.e., GPP (Figure 2) at DBF and CL sites once the land surface is clear of snow and wetness. However, the method has not been previously applied and validated in ENF forests, and, as Figure 2 shows, the NDII approach fails to capture the SOS and EOS trends due to the intermittent green-up of needleleaf forest with snowmelt. Other studies which used NDII found that in certain cases the onset of vegetation growth could not be retrieved, since snowmelt did not exactly follow the pattern of vegetation growth [*de Beurs and Henebry*, 2010; *Peckham et al.*, 2008]. If snowmelt and green-up overlap for a long period, the NDII methodology could estimate the green-up to occur later than the observed onset of green-up in the field [*Delbart et al.*, 2005]. Figure 2 also shows the lack of any significant NDII trends in needleleaf forest which are relevant for SOS and EOS extraction. In addition to this, NDII has a very small dynamic range (Figure 2). Finally, the NDII of snow or a wet landscape can be comparable or higher to that of a vegetated surface even in DBF, which creates problems if NDII is applied over a large area where land cover information is not available. This can also be confused with seasonal land surface moisture dynamics, as most of the world's forests grow in seasonally distinct rainfall cycles.

[29] The new phenology index, PI, developed in this study combines the strength of NDVI and NDII and largely follows the GPP trend (Figure 2 and Figure 4). Some disagreements between the PI- and GPP-based estimates can be explained by the possible missing or poor quality remote sensing observations during the transition periods of LSP, and the lag between optically measurable greenness increase and photosynthesis. One should note also that we have used only one tower flux site pixel (0.25 km^2). As such, particularly at less productive sites, the tower GPP can be affected by variably greening or browning surrounding vegetation which may mask the small signal observed at a target site.

[30] Generally speaking, unlike most previous studies which focus on deciduous vegetation LSP, we have tried to estimate LSP DOYs of ENF flux tower sites which posed several challenges. Despite these challenges, we have successfully implemented phenology metrics to CO_2 flux measurements, which can be incorporated with remote sensing footprints for LSP estimates. GPP provides an objective measure of SOS and EOS. We have also implemented the double logistic method to estimate SOS and EOS from GPP, with a new approach for extracting the start and the end of the transition of the SOS and EOS. The new estimates of SOS and EOS from the start and end of the transition slopes provide objective measures for other phenology studies. Another emerging and promising approach for LSP observation is the increasing availability of networks of web cameras [*Richardson et al.*, 2009] that match LSP validation from remote sensing footprint rather than the traditional individual plant phenology networks. The LSP, compared to individual plant or plant organ phenology cycles, integrates the collective effects of atmospheric, environmental, and edaphic conditions and interspecific responses to the changing climate.

[31] The caveat of the proposed PI-based method is the lack of long-term remote sensing observations as coarse resolution satellite sensors with SWIR spectral band only emerged in the late 1990s. However, given the future development direction of earth observation satellites and the growing archive of existing data, the PI will be a valuable index for LSP studies.

[32] Finally, LSP studies are currently debating methods and controversial claims such as the one on the green-up of the Amazon forest during the dry season [*Huete et al.*, 2006; *Saleska et al.*, 2007; *Samanta et al.*, 2010; *Soudani et al.*, 2012; *Xiao et al.*, 2006]. There are also evolving developments in LSP methods, such as ground networks of webcams [*Migliavacca et al.*, 2011; *Richardson et al.*, 2009; *Richardson et al.*, 2007; *Sonnentag et al.*, 2012], ground-based spectral measurements [*Soudani et al.*, 2012], the use of MODIS standard LSP products based on enhanced vegetation index (EVI) [*Ganguly et al.*, 2010], and ground-based photosynthetic radiation measurements [*Richardson et al.*, 2012], which are expected to help extract the subtle LSP interannual and spatial variability across plant functional types. However, there are several limitations in all of these methods. Alternative approaches such as the use of several indicators as presented here in the form of difference of squared greenness and wetness, and other LSP proxies which can decouple the wetness and brightness temporal trends from vegetation development should be encouraged. The classical approach of using a single LSP indicator has often led to controversial claims [*Samanta et al.*, 2010; *White et al.*, 2009].

6. Conclusions

[33] Using 83 site-years deciduous broadleaf and evergreen needleleaf forests and croplands across North America's temperate and boreal vegetation from Canadian Carbon

Figure 9. Interannual variation of growing season length plotted along each year, as estimated from normalized difference vegetation index (NDVI), indicated by crosses; phenology index (PI), indicated by solid circles; and gross primary production (GPP), indicated by open circles. Top panel is for evergreen needleleaf forest, middle panel is for deciduous broadleaf forest, and bottom panel is for cropland. (a) CA-EOBS, (b) CA-SOBS, (c) CA-NOBS, (d) U.S.-WCR, (e) U.S.-MMS, (f) CA-OA, (g) U.S.-UMB, (h) U.S.-Los, (i) U.S.-NE1, (j) U.S.-NE2, and (k) U.S.-NE3. Descriptions of CO_2 flux tower sites are given in Table 1.

Program and AmeriFlux CO_2 flux networks measurements, we have successfully implemented a new phenology index (PI) for LSP estimations. PI is essentially the difference of squared greenness and wetness during growing season. We have also successfully compared the SOS and EOS estimates from remote sensing observations with GPP-based LSP estimates. Generally speaking, PI estimates the SOS and EOS dates better than NDVI compared to LSP estimates from GPP measurements. Our results indicate that not only the start but also the end of growing season can be estimated using remote sensing observations. The implication of our study is that, LSP metrics from remote sensing methods either should employ larger spectral information available in most coarse resolution satellite sensors or use a combination of several vegetation indices. This is needed to disentangle the seasonal dynamics of wetness (surface moisture) and brightness (background soil) from greenness cycles.

[34] Based on our findings and previous works [*Gu et al.*, 2003; *Gu et al.*, 2009; *Richardson et al.*, 2010; *Xiao et al.*, 2009], we encourage the cooperation of remote sensing and CO_2 flux communities in order to extensively use the remote sensing observations and more than 600 CO_2 flux tower measurements across various biomes in the world. PI needs further validation, particularly in moisture limited ecosystem with tropical and subtropical vegetation. Future work should also look into the comparative analysis of remote sensing LSP metrics from NDVI, EVI, PI, Photochemical reflectance index (PRI), and ground-based photosynthetic radiation observations in comparison with reference measures such as GPP- and webcam-based LSP estimates, and citizen science plant-watch networks with proper spatial scaling.

[35] **Acknowledgments.** This study was supported by an NSERC Strategic Grant (STPGP 381474–09). We thank the AmeriFlux and Fluxnet-Canada (Canadian Carbon Program) networks; the site principal investigators, co-investigators, participants, and data collection and processing staff for contributing to the tower flux data; and the agencies and institutions that funded long-term measurements at these sites. Flux observations at U.S.-WCr were made possible by support from the Department of Energy (DOE) National Institute for Global Environmental Change and Wisconsin Focus on Energy EERD 10–06 and at U.S.-Los by the DOE Office of Biological and Environmental Research (BER) National Institute for Climatic Change Research (NICCR) Midwestern Region Subagreement 050516Z19. We thank the MODIS land product processing team at Oak Ridge National Laboratory Distributed Active Archive Center (ORNL DAAC) for the MODIS Collection 5 data. We thank Ankur R. Desai for comments on an earlier version of the manuscript. Two anonymous reviewers, the Editor, and Associate Editor all provided valuable comments.

References

Alcaraz-Segura, D., E. Chuvieco, H. E. Epstein, E. S. Kasischke, and A. Trishchenko (2010), Debating the greening vs. browning of the North American boreal forest: Differences between satellite datasets, *Global Change Biol.*, *16*(2), 760–770, doi:10.1111/j.1365-2486.2009.01956.x.

Baldridge, A. M., S. J. Hook, C. I. Grove, and G. Rivera (2009), The ASTER spectral library version 2.0, *Remote Sens. Environ.*, *113*(4), 711–715, doi:10.1016/j.rse.2008.11.007.

Barr, A. G., T. A. Black, E. H. Hogg, N. Kljun, K. Morgenstern, and Z. Nesic (2004), Inter-annual variability in the leaf area index of a boreal aspen-hazelnut forest in relation to net ecosystem production, *Agric. For. Meteorol.*, *126*(3–4), 237–255, doi:10.1016/j.agrformet.2004.06.011.

Bergeron, O., H. A. Margolis, T. A. Black, C. Coursolle, A. L. Dunn, A. G. Barr, and S. C. Wofsy (2007), Comparison of carbon dioxide fluxes over three boreal black spruce forests in Canada, *Global Change Biol.*, *13*(1), 89–107, doi:10.1111/j.1365-2486.2006.01281.x.

Bradley, A. V., F. F. Gerard, N. Barbier, G. P. Weedon, L. O. Anderson, C. Huntingford, L. E. O. C. Aragao, P. Zelazowski, and E. Arai (2011), Relationships between phenology, radiation and precipitation in the Amazon region, *Global Change Biol.*, *17*(6), 2245–2260, doi:10.1111/j.1365-2486.2011.02405.x.

Brown, L., J. M. Chen, S. G. Leblanc, and J. Cihlar (2000), A shortwave infrared modification to the simple ratio for LAI retrieval in boreal forests: An image and model analysis, *Remote Sens. Environ.*, *71*(1), 16–25, doi:10.1016/S0034-4257(99)00035-8.

Brown, M. E., K. de Beurs, and A. Vrieling (2010), The response of African land surface phenology to large scale climate oscillations, *Remote Sens. Environ.*, *114*(10), 2286–2296, doi:10.1016/j.rse.2010.05.005.

Bunn, A. G., and S. J. Goetz (2006), Trends in satellite-observed circumpolar photosynthetic activity from 1982 to 2003: The influence of seasonality, cover type, and vegetation density, *Earth Interact.*, *10*, 1–19, doi:10.1175/EI190.1.

Chen, B., T. A. Black, N. C. Coops, T. Hilker, J. A. Trofymow, and K. Morgenstern (2009), Assessing tower flux footprint climatology and scaling between remotely sensed and eddy covariance measurements, *Boundary Layer Meteorol.*, *130*(2), 137–167, doi:10.1007/s10546-008-9339-1.

Cleland, E. E., I. Chuine, A. Menzel, H. A. Mooney, and M. D. Schwartz (2007), Shifting plant phenology in response to global change, *Trends Ecol. Evol.*, *22*(7), 357–365, doi:10.1016/j.tree.2007.04.003.

Cook, B. D., et al. (2004), Carbon exchange and venting anomalies in an upland deciduous forest in northern Wisconsin, USA, *Agric. For. Meteorol.*, *126*(3–4), 271–295, doi:10.1016/j.agrformet.2004.06.008.

Coppin, P. R., and M. E. Bauer (1994), Processing of multitemporal Landsat TM imagery to optimize extraction of forest cover change features, *IEEE Trans. Geosci. Remote Sens.*, *32*(4), 918–927, doi:10.1109/36.298020.

de Beurs, K. M., and G. M. Henebry (2004), Land surface phenology, climatic variation, and institutional change: Analyzing agricultural land cover change in Kazakhstan, *Remote Sens. Environ.*, *89*(4), 497–509, doi:10.1016/j.rse.2003.11.006.

de Beurs, K. M., and G. M. Henebry (2008), Northern annular mode effects on the land surface phenologies of northern Eurasia, *J. Clim.*, *21*(17), 4257–4279, doi:10.1175/2008JCLI2074.1.

de Beurs, K. M., and G. M. Henebry (2010), A land surface phenology assessment of the northern polar regions using MODIS reflectance time series, *Can. J. Rem. Sens.*, *36*, S87–S110, doi:10.5589/m10-021.

Delbart, N., L. Kergoat, T. Le Toan, J. Lhermitte, and G. Picard (2005), Determination of phenological dates in boreal regions using normalized difference water index, *Remote Sens. Environ.*, *97*(1), 26–38, doi:10.1016/j.rse.2005.03.011.

Delbart, N., T. Le Toan, L. Kergoat, and V. Fedotova (2006), Remote sensing of spring phenology in boreal regions: A free of snow-effect method using NOAA-AVHRR and SPOT-VGT data (1982–2004), *Remote Sens. Environ.*, *101*(1), 52–62, doi:10.1016/j.rse.2005.11.012.

Delbart, N., G. Picard, T. Le Toans, L. Kergoat, S. Quegan, I. Woodward, D. Dye, and V. Fedotova (2008), Spring phenology in boreal Eurasia over a nearly century time scale, *Global Change Biol.*, *14*(3), 603–614, doi:10.1111/j.1365-2486.2007.01505.x.

Dragoni, D., H. P. Schmid, C. A. Wayson, H. Potter, C. S. B. Grimmond, and J. C. Randolph (2011), Evidence of increased net ecosystem productivity associated with a longer vegetated season in a deciduous forest in south-central Indiana, USA, *Global Change Biol.*, *17*(2), 886–897, doi:10.1111/j.1365-2486.2010.02281.x.

Dunn, A. L., C. C. Barford, S. C. Wofsy, M. L. Goulden, and B. C. Daube (2007), A long-term record of carbon exchange in a boreal black spruce forest: Means, responses to interannual variability, and decadal trends, *Global Change Biol.*, *13*(3), 577–590, doi:10.1111/j.1365-2486.2006.01221.x.

Dye, D. G., and C. J. Tucker (2003), Seasonality and trends of snow-cover, vegetation index, and temperature in northern Eurasia, *Geophys. Res. Lett.*, *30*(7), 1405, doi:10.1029/2002GL016384.

Fisher, J. I., J. F. Mustard, and M. A. Vadeboncoeur (2006), Green leaf phenology at Landsat resolution: Scaling from the field to the satellite, *Remote Sens. Environ.*, *100*(2), 265–279, doi:10.1016/j.rse.2005.10.022.

Fitter, A. H., and R. S. R. Fitter (2002), Rapid changes in flowering time in British plants, *Science*, *296*(5573), 1689–1691, doi:10.1126/science.1071617.

Frolking, S., K. C. McDonald, J. S. Kimball, J. B. Way, R. Zimmermann, and S. W. Running (1999), Using the space-borne NASA scatterometer (NSCAT) to determine the frozen and thawed seasons, *J. Geophys. Res.*, *104*(D22), 27,895–27,907, doi:10.1029/1998JD200093.

Ganguly, S., M. A. Friedl, B. Tan, X. Zhang, and M. Verma (2010), Land surface phenology from MODIS: Characterization of the Collection 5 global land cover dynamics product, *Remote Sens. Environ.*, *114*(8), 1805–1816, doi:10.1016/j.rse.2010.04.005.

Goetz, S. J., A. G. Bunn, G. J. Fiske, and R. A. Houghton (2005), Satellite-observed photosynthetic trends across boreal North America associated with climate and fire disturbance, *Proc. Natl. Acad. Sci. U. S. A.*, *102*(38), 13,521–13,525, doi:10.1073/pnas.0506179102.

Gonsamo, A. (2011), Normalized sensitivity measures for leaf area index estimation using three-band spectral vegetation indices, *Int. J. Remote Sens.*, *32*(7), 2069–2080, doi:10.1080/01431161.2010.502153.

Gonsamo, A., J. M. Chen, C. Wu, and D. Dragoni (2012), Predicting deciduous forest carbon uptake phenology by upscaling FLUXNET measurements using remote sensing data, *Agric. For. Meteorol.*, *165*, 127–135, doi:10.1016/j.agrformet.2012.06.006.

Gonsamo, A., and P. Pellikka (2012), The sensitivity-based estimation of leaf area index from spectral vegetation indices, *ISPRS J. Photogramm. Remote Sens.*, *70*(0), 15–25, doi:10.1016/j.isprsjprs.2012.03.009.

Gu, L., W. M. Post, D. Baldocchi, T. A. Black, S. B. Verma, T. Vesala, and S. C. Wofsy (2003), Phenology of vegetation photosynthesis, in *Phenology: An Integrated Environmental Science*, edited by M. D. Schwartz, pp. 467–485, Kluwer, Dordecht, Netherlands, doi:10.1007/978-94-007-0632-3_29.

Gu, L., W. M. Post, D. D. Baldocchi, T. A. Black, A. E. Suyker, S. B. Verma, T. Vesala, and S. C. Wofsy (2009), Characterizing the seasonal dynamics of plant community photosynthesis across a range of vegetation types, in *Phenology of Ecosystem Processes: Applications in Global Change Research*, edited by A. Noormets, pp. 35–58, Springer, New York, doi:10.1007/978-1-4419-0026-5_2.

Harazono, Y., M. Mano, A. Miyata, R. C. Zulueta, and W. C. Oechel (2003), Inter-annual carbon dioxide uptake of a wet sedge tundra ecosystem in the Arctic, *Tellus, Ser. B*, *55*(2), 215–231, doi:10.1034/j.1600-0889.2003.00012.x.

Hardisky, M. A., V. Klemas, and R. M. Smart (1983), The influences of soil salinity, growth form, and leaf moisture on the spectral reflectance of *Spartina alterniflora* canopies, *Photogramm. Eng. Remote Sens.*, *49*, 77–83.

Dunn, A. H., and K. M. de Beurs (2011), Land surface phenology of North American mountain environments using moderate resolution imaging spectroradiometer data, *Remote Sens. Environ.*, *115*(5), 1220–1233, doi:10.1016/j.rse.2011.01.005.

Huete, A. R., and R. D. Jackson (1988), Soil and atmosphere influences on the spectra of partial canopies, *Remote Sens. Environ.*, *25*(1), 89–105, doi:10.1016/0034-4257(88)90043-0.

Huete, A., C. Justice, and H. Liu (1994), Development of vegetation and soil indices for MODIS-EOS, *Remote Sens. Environ.*, *49*(3), 224–234, doi:10.1016/0034-4257(94)90018-3.

Huete, A. R., H. Q. Liu, K. Batchily, and W. vanLeeuwen (1997), A comparison of vegetation indices global set of TM images for EOS-MODIS, *Remote Sens. Environ.*, *59*(3), 440–451, doi:10.1016/S0034-4257(96)00112-5.

Huete, A., K. Didan, T. Miura, E. P. Rodriguez, X. Gao, and L. G. Ferreira (2002), Overview of the radiometric and biophysical performance of the MODIS vegetation indices, *Remote Sens. Environ.*, *83*(1–2), 195–213, doi:10.1016/S0034-4257(02)00096-2.

Huete, A. R., K. Didan, Y. E. Shimabukuro, P. Ratana, S. R. Saleska, L. R. Hutyra, W. Z. Yang, R. R. Nemani, and R. Myneni (2006), Amazon rainforests green-up with sunlight in dry season, *Geophys. Res. Lett.*, *33*, L06405, doi:10.1029/2005GL025583.

Intergovernmental Panel on Climate Change (2007), *Climate Change 2007: The Physical Science Basis. Contribution of Working Group I to the Fourth Assessment Report of the Intergovernmental Panel on Climate Change*, edited by S. Solomon, et al., Cambridge Univ. Press, Cambridge, U. K.

Jarvis, P., and S. Linder (2000), Botany: Constraints to growth of boreal forests, *Nature*, *405*(6789), 904–905, doi:10.1038/35016154.

Jeong, S.-J., D. Medvigy, E. Shevliakova, and S. Malyshev (2012), Uncertainties in terrestrial carbon budgets related to spring phenology, *J. Geophys. Res.*, *117*, G01030, doi:10.1029/2011JG001868.

Liang, L., M. D. Schwartz, and S. Fei (2011), Validating satellite phenology through intensive ground observation and landscape scaling in a mixed seasonal forest, *Remote Sens. Environ.*, *115*(1), 143–157, doi:10.1016/j.rse.2010.08.013.

Lieth, H. (1974), *Phenology and Seasonality Modeling*, 444 pp., Springer, New York.

McDonald, K. C., J. S. Kimball, E. Njoku, R. Zimmermann, and M. Zhao (2004), Variability in springtime thaw in the terrestrial high latitudes: Monitoring a major control on the biospheric assimilation of atmospheric CO_2 with spaceborne microwave remote sensing, *Earth Interact.*, *8*, 1–23, doi:10.1175/1087-3562(2004)8<1:VISTIT>2.0.CO;2.

Menzel, A., and P. Fabian (1999), Growing season extended in Europe, *Nature*, *397*(6721), 659, doi:10.1038/17709.

Menzel, A., et al. (2006), European phenological response to climate change matches the warming pattern, *Global Change Biol.*, *12*(10), 1969–1976, doi:10.1111/j.1365-2486.2006.01193.x.

Migliavacca, M., et al. (2011), Using digital repeat photography and eddy covariance data to model grassland phenology and photosynthetic CO_2 uptake, *Agric. For. Meteorol.*, *151*(10), 1325–1337, doi:10.1016/j.agrformet.2011.05.012.

Morisette, J. T., et al. (2009), Tracking the rhythm of the seasons in the face of global change: Phenological research in the 21st century, *Front. Ecol. Environ*, *7*(5), 253–260, doi:10.1890/070217.

Myneni, R. B., C. D. Keeling, C. J. Tucker, G. Asrar, and R. R. Nemani (1997), Increased plant growth in the northern high latitudes from 1981 to 1991, *Nature*, *386*(6626), 698–702, doi:10.1038/386698a0.

Nave, L. E., et al. (2011), Disturbance and the resilience of coupled carbon and nitrogen cycling in a north temperate forest, *J. Geophys. Res.*, *116*, G04016, doi:10.1029/2011JG001758.

Noormets, A., J. Chen, L. Gu, and A. R. Desai (2009), The phenology of gross ecosystem productivity and ecosystem respiration in temperate hardwood and conifer chronosequences, in *Phenology of Ecosystem Processes: Applications in Global Change Research*, edited by A. Noormets, pp. 59–85, Springer, New York, doi:10.1007/978-1-4419-0026-5_3.

Parmesan, C. (2006), Ecological and evolutionary responses to recent climate change, *Annu. Rev. Ecol. Evol. Syst.*, *37*, 637–669, doi:10.1146/annurev.ecolsys.37.091305.110100.

Peckham, S. D., D. E. Ahl, S. P. Serbin, and S. T. Gower (2008), Fire-induced changes in green-up and leaf maturity of the Canadian boreal forest, *Remote Sens. Environ.*, *112*(9), 3594–3603, doi:10.1016/j.rse.2008.04.016.

Piao, S., P. Friedlingstein, P. Ciais, N. Viovy, and J. Demarty (2007), Growing season extension and its impact on terrestrial carbon cycle in the Northern Hemisphere over the past 2 decades, *Global Biogeochem. Cycles*, *21*, GB3018, doi:10.1029/2006GB002888.

Piao, S., et al. (2008), Net carbon dioxide losses of northern ecosystems in response to autumn warming, *Nature*, *451*(7174), 49–52, doi:10.1038/nature06444.

Reed, B. C. (2006), Trend analysis of time-series phenology of North America derived from satellite data, *GISci. Remote Sens.*, *43*(1), 24–38, doi:10.2747/1548-1603.43.1.24.

Reichstein, M., et al. (2005), On the separation of net ecosystem exchange into assimilation and ecosystem respiration: Review and improved algorithm, *Global Change Biol.*, *11*(9), 1424–1439, doi:10.1111/j.1365-2486.2005.001002.x.

Richardson, A. D., J. P. Jenkins, B. H. Braswell, D. Y. Hollinger, S. V. Ollinger, and M.-L. Smith (2007), Use of digital webcam images to track spring green-up in a deciduous broadleaf forest, *Oecologia*, *152*(2), 323–334, doi:10.1007/s00442-006-0657-z.

Richardson, A. D., B. H. Braswell, D. Y. Hollinger, J. P. Jenkins, and S. V. Ollinger (2009), Near-surface remote sensing of spatial and temporal variation in canopy phenology, *Ecol. Appl.*, *19*(6), 1417–1428, doi:10.1890/08-2022.1.

Richardson, A. D., et al. (2010), Influence of spring and autumn phenological transitions on forest ecosystem productivity, *Philos. Trans. R. Soc. London, Ser. B*, *365*(1555), 3227–3246, doi:10.1098/rstb.2010.0102.

Richardson, A. D., et al. (2012), Terrestrial biosphere models need better representation of vegetation phenology: Results from the North American Carbon Program Site Synthesis, *Global Change Biol.*, *18*, 566–584, doi:10.1111/j.1365-2486.2011.02562.x.

Roy, D. B., and T. H. Sparks (2000), Phenology of British butterflies and climate change, *Global Change Biol.*, *6*(4), 407–416, doi:10.1046/j.1365-2486.2000.00322.x.

Sakamoto, T., B. D. Wardlow, A. A. Gitelson, S. B. Verma, A. E. Suyker, and T. J. Arkebauer (2010), A Two-Step Filtering approach for detecting maize and soybean phenology with time-series MODIS data, *Remote Sens. Environ.*, *114*(10), 2146–2159, doi:10.1016/j.rse.2010.04.019.

Saleska, S. R., K. Didan, A. R. Huete, and H. R. da Rocha (2007), Amazon forests green-up during 2005 drought, *Science*, *318*(5850), 612, doi:10.1126/science.1146663.

Samanta, A., S. Ganguly, H. Hashimoto, S. Devadiga, E. Vermote, Y. Knyazikhin, R. R. Nemani, and R. B. Myneni (2010), Amazon forests did not green-up during the 2005 drought, *Geophys. Res. Lett.*, *37*, L05401, doi:10.1029/2009GL042154.

Schwartz, M. D. (1998), Green-wave phenology, *Nature*, *394*(6696), 839–840, doi:10.1038/29670.

Schwartz, M. D., and J. M. Hanes (2010), Intercomparing multiple measures of the onset of spring in eastern North America, *Int. J. Climatol.*, *30*, 1614–1626, doi:10.1002/joc.2008.

Schwartz, M. D., and B. E. Reiter (2000), Changes in North American spring, *Int. J. Climatol.*, *20*(8), 929–932, doi:10.1002/1097-0088(20000630)20:8<929::AID-JOC557>3.0.CO;2–5.

Shabanov, N. V., L. M. Zhou, Y. Knyazikhin, R. B. Myneni, and C. J. Tucker (2002), Analysis of interannual changes in northern vegetation activity observed in AVHRR data from 1981 to 1994, *IEEE Trans. Geosci. Remote Sens.*, *40*(1), 115–130, doi:10.1109/36.981354.

Sonnentag, O., K. Hufkens, C. Teshera-Sterne, A. M. Young, M. Friedl, B. H. Braswell, T. Milliman, J. O'Keefe, and A. D. Richardson (2012), Digital repeat photography for phenological research in forest ecosystems, *Agric. For. Meteorol.*, *152*(0), 159–177, doi:10.1016/j.agrformet.2011.09.009.

Soudani, K., et al. (2012), Ground-based network of NDVI measurements for tracking temporal dynamics of canopy structure and vegetation phenology in different biomes, *Remote Sens. Environ.*, *123*(0), 234–245, doi:10.1016/j.rse.2012.03.012.

Sulman, B. N., A. R. Desai, B. D. Cook, N. Saliendra, and D. S. Mackay (2009), Contrasting carbon dioxide fluxes between a drying shrub wetland in Northern Wisconsin, USA, and nearby forests, *Biogeosciences*, *6*(6), 1115–1126, doi:10.5194/bg-6-1115-2009.

Verma, S. B., et al. (2005), Annual carbon dioxide exchange in irrigated and rainfed maize-based agroecosystems, *Agric. For. Meteorol.*, *131*(1–2), 77–96, doi:10.1016/j.agrformet.2005.05.003.

Vermote, E. F., and A. Vermeulen (1999), Atmospheric correction algorithm: Spectral reflectances (MOD09), Version 4.0, 107 pp., NASA, Greenbelt, Md. [Available at http://modis.gsfc.nasa.gov/data/atbd/atbd_mod08.pdf.]

Walther, G. R., E. Post, P. Convey, A. Menzel, C. Parmesan, T. J. C. Beebee, J. M. Fromentin, O. Hoegh-Guldberg, and F. Bairlein (2002), Ecological responses to recent climate change, *Nature*, *416*(6879), 389–395, doi:10.1038/416389a.

White, M. A., S. W. Running, and P. E. Thornton (1999), The impact of growing-season length variability on carbon assimilation and evapotranspiration over 88 years in the eastern US deciduous forest, *Int. J. Biometeorol.*, *42*(3), 139–145, doi:10.1007/s004840050097.

White, M. A., et al. (2009), Intercomparison, interpretation, and assessment of spring phenology in North America estimated from remote sensing for 1982–2006, *Global Change Biol.*, *15*(10), 2335–2359, doi:10.1111/j.1365-2486.2009.01910.x.

Wu, C., J. M. Chen, A. Gonsamo, D. T. Price, A. Black, and W. A. Kurz (2012), Interannual variability of net carbon exchange is related to the lag between the end-dates of net carbon uptake and photosynthesis: Evidence from long records at two contrasting forest stands, *Agric. For. Meteorol.*, *164*, 29–38, doi:10.1016/j.agrformet.2012.05.002.

Xiao, X., S. Hagen, Q. Zhang, M. Keller, and B. Moore III (2006), Detecting leaf phenology of seasonally moist tropical forests in South America with multi-temporal MODIS images, *Remote Sens. Environ.*, *103*(4), 465–473, doi:10.1016/j.rse.2006.04.013.

Xiao, X., J. Zhang, H. Yan, W. Wu, and C. Biradar (2009), Land surface phenology: Convergence of satellite and CO_2 eddy flux observations, in *Phenology of Ecosystem Processes: Applications in Global Change Research*, edited by A. Noormets, pp. 247–270, Springer, New York, doi:10.1007/978-1-4419-0026-5_11.

Zhang, X., D. Tarpley, and J. T. Sullivan (2007), Diverse responses of vegetation phenology to a warming climate, *Geophys. Res. Lett.*, *34*, L19405, doi:10.1029/2007GL031447.